TURUN YLIOPISTON JULKAISUJA
ANNALES UNIVERSITATIS TURKUENSIS

SARJA - SER. A I OSA - TOM. 399

ASTRONOMICA - CHEMICA - PHYSICA - MATHEMATICA

ON TOPOLOGICAL SOLITONS IN THE FADDEEV-SKYRME MODEL AND ITS EXTENSIONS

by

Juha Jäykkä

TURUN YLIOPISTO
Turku 2009

From

Department of Physics and Astronomy
University of Turku
Finland

Supervised by

Jarmo Hietarinta
Professor of Theoretical Physics
Department of Physics and Astronomy
University of Turku
Finland

Reviewed by

Luiz Ferreira
Professor
Instituto de Fisica de Sao Carlos
Depto. de Fisica e Ciencias dos Materiais
Brazil

Antti Niemi
Professor of Theoretical Physics
Department of Physics and Astronomy
Uppsala University
Sweden

Opponent

Wojciech J. Zakrzewski
Professor of Mathematics
Centre for Particle Theory
Durham University
United Kingdom

ISBN 978-951-29-3964-0 (PRINT)
ISBN 978-951-29-3965-7 (PDF)
ISSN 0082-7002
Painosalama Oy – Turku, Finland 2009

Acknowledgements

This work is based on research which has been carried out in the Department of Physics and Astronomy in the University of Turku. I would like to express my gratitude for all the personnel at the Laboratory of Theoretical Physics for the superb working atmosphere. My special thanks go to my supervisors Prof. Jarmo Hietarinta and Doc. Petri Salo (Helsinki University of Technology) for their instructions, advice and unwavering belief that this work will eventually be finished. I would also like to thank Dr. Tuomas Multamäki and Dr. Matti Ropo for countless relaxing discussions.

I want to acknowledge the financial support of this work by research grants from the Academy of Finland (projects 47188 and 123311) and the Jenny and Antti Wihuri Foundation. The generous computer resources of the M-grid project and CSC – IT Center for Science Ltd are also acknowledged.

Finally, I want to express my deepest gratitude to my beloved wife, Linda for her understanding and love.

Contents

Abstract

The topological solitons of two classical field theories, the Faddeev-Skyrme model and the Ginzburg-Landau model are studied numerically and analytically in this work. The aim is to gain information on the existence and properties of these topological solitons, their structure and behaviour under relaxation.

First, the conditions and mechanisms leading to the possibility of topological solitons are explored from the field theoretical point of view. This leads one to consider continuous deformations of the solutions of the equations of motion. The results of algebraic topology necessary for the systematic treatment of such deformations are reviewed and methods of determining the homotopy classes of topological solitons are presented.

The Faddeev-Skyrme and Ginzburg-Landau models are presented, some earlier results reviewed and the numerical methods used in this work are described.

The topological solitons of the Faddeev-Skyrme model, Hopfions, are found to follow the same mechanisms of relaxation in three different domains with three different topological classifications. For two of the domains, the necessary but unusual topological classification is presented.

Finite size topological solitons are not found in the Ginzburg-Landau model and a scaling argument is used to suggest that there are indeed none unless a certain modification to the model, due to R. S. Ward, is made. In that case, the Hopfions of the Faddeev-Skyrme model are seen to be present for some parameter values. A boundary in the parameter space separating the region where the Hopfions exist and the area where they do not exist is found and the behaviour of the Hopfion energy on this boundary is studied.

List of papers

This thesis consists of a review of the subject and the following original research articles

I J. Hietarinta, J. Jäykkä, and P. Salo, Dynamics of vortices and knots in Faddeev's model, in *Workshop on Integrable Theories, Solitons and Duality* (2002), PoS(unesp2002)017

II J. Hietarinta, J. Jäykkä, and P. Salo, Relaxation of twisted vortices in the Faddeev-Skyrme model, Phys. Lett. **A321**, 324 (2004), `cond-mat/0309499`.

III J. Jäykkä, J. Hietarinta, and P. Salo, Topologically nontrivial configurations associated with Hopf charges investigated in the two-component Ginzburg-Landau, Phys. Rev. **B77**, 094509 (2008), `cond-mat/0608424`.

IV J. Jäykkä, Stability of topological solitons in modified two-component Ginzburg-Landau model Phys. Rev. **D79**, 065006 (2009), `arXiv:0901.4579`.

V J. Jäykkä and J. Hietarinta, Unwinding in Hopfion vortex bunches, preprint, `arXiv:0904.1305v1` (2009).

Chapter 1

Introduction

In this work, the existence and properties of *topological solitons* in certain physical models is studied. The idea of topological solitons is very old. Perhaps the earliest attempt of using topological concepts to describe physical objects was the knotted vortex model of atoms by Lord Kelvin [1]. While he did not use the term topological soliton, his model is still considered a precursor of modern theories with topological solitons. Another precursor is the Dirac monopole [2, 3], where the usual model of the electromagnetic field is modified so that it contains magnetic poles. The Dirac monopole is not a proper topological soliton because the pole itself is singular, but nevertheless the field configuration very far from the pole has a non-trivial topology, which defines a topological invariant. The topological invariant of the model is interpreted as the magnetic charge of the monopole.

With the advent of Abrikosov vortices [4] in superconductors and the Skyrme model [5, 6, 7, 8], modern research into topological solitons had begun. After these, many other topological solitons were considered, mostly in particle physics, like the monopole of 't Hooft and Polyakov [9, 10], the dyon of Julia and Zee [11] and the knot soliton of Faddeev [12], which is often called a Hopfion. By the 1980's, the field of topological solitons, or defects as they were often called, had established itself as an important source of descriptions and candidate explanations for things like the matter distribution of the universe [13], quark confinement [14], defects in liquid crystals [15] and some properties of the superfluid phase of liquid helium [16], ferromagnets [17] and superconductors [4]. Topological solitons are also present in supersymmetric models [18]. The problem, however, is that rigorous mathematical analysis of topological solitons is currently severely limited: analytical solutions are known for very few models – two such examples will be presented in Section 2.3. Therefore, numerical investigation

is necessary. The problem is of such complexity, that the numerical capabilities have only recently become sufficient for a detailed analysis of many of the models, including those studied here.

Creating topological solitons is now common routine in many laboratories, even though some of the models with topological solitons are not experimentally realisable, like the early universe. For example, the defects in nematic liquid crystals [19] have been studied experimentally for quite some time, and Abrikosov vortices have been studied for decades [20]. The topological solitons have been found to have a profound effect on the properties of the material in which they occur. Vortices in Bose-Einstein condensates [21] and superfluid helium [16, 22, 23, 24] are now also routinely observed. The number of new situation where topological solitons are observed is continually expanding with new cases [25, 26].

The multitude of laboratory experiments prompt the important question of theoretical modelling of topological solitons. Therefore it is necessary to study in detail the basic theories with topological solitons, in order to be able to apply this knowledge to more realistic models and perhaps propose experiments where they can be observed and their effect and relevance appreciated. Due to difficulties related to obtaining analytical solutions, it is necessary to use numerical methods and this is the main content of the work at hand.

One very interesting case is the Faddeev-Skyrme model [12] studied in this work. It is the simplest (known) three dimensional model which supports topological solitons and it is known to exist as a limit of some more complicated or realistic models [27]. There are connections with the Faddeev-Skyrme model and the way hadrons combine into more complicated structures such as protons and nuclei [14, 28]. The Faddeev-Skyrme model can also be embedded into the other model studied in this work, the Ginzburg-Landau model [29], which is the model behind perhaps the most famous topological solitons, the Abrikosov vortices. Therefore, studying the Faddeev-Skyrme and Ginzburg-Landau models in detail provides invaluable insight into the properties of topological solitons.

This work is arranged as follows. In Chapter 2 the concepts of classical field theory are introduced and two examples are given. These give physical motivation for the use of the topological concepts and properties covered in Chapter 3, where the term *topological soliton* is defined and the most relevant results from topology are reviewed without reference to any specific physical model. In Chapter 4 the results of Chapter 3 are applied

to the physical models investigated in this work. The numerical methods are described in Chapter 5 and the results and conclusions of the original publications are presented in Chapters 6 and 7. The notations chosen in this work mostly follow the usual conventions of theoretical physics and are summarised in Appendix A. The original publications are reprinted at the end (Papers I-V, corresponding to [30, 31, 32, 33, 34], respectively).

Chapter 2

Classical field theory

This work studies topological solitons solely in the classical context. A *classical field* is a set of values defined at all points of the relevant physical space, for example the temperature in a room, the wind velocities of a cyclone or the electromagnetic field. A more complicated example would be the general theory of relativity. The physical space is denoted by $\mathcal{P}$ in this work and will usually be $\mathbb{R}^3$. The values of the field are usually either $\mathbb{R}^n$ or $\mathbb{C}^n$ or subsets thereof. The set of values in the first three examples above belong to $\mathbb{R}$, $\mathbb{R}^3$ and $\mathbb{R}^4$; the set of possible values is called the *configuration space* and is here denoted by $\mathcal{C}$. The field itself is then a mapping $f : \mathcal{P} \to \mathcal{C}$. As the variety of examples suggests, classical fields are prevalent throughout theoretical physics, even though the theories are not always treated as field theories. The notable exceptions, where classical fields are absent, are quantum physics and Newtonian mechanics of a finite number of point particles or rigid bodies. (However, the classical theory of fields can be obtained from the Newtonian mechanics in the limit of an infinite number of particles.)

2.1 Classical field and Euler-Lagrange equations

The basic objects of a classical field theory are the field f, the physical space $\mathcal{P}$, the configuration space $\mathcal{C}$ and a function called the *Lagrangian density*, which gives the dynamics of the theory. The field is a function $f : \mathcal{P} \to \mathcal{C}$ and the fields in this work are assumed to be smooth. The Lagrangian density is a function of the field f and its time and space derivatives as follows.

Definition 2.1 (Lagrangian density)**.** Let $f : \mathcal{P} \to \mathcal{C}$ be a classical field and $\mathcal{L}$ a function of f and its derivatives. If the function $\mathcal{L}$

i) is an analytic function of the field f,

ii) is a polynomial of the space derivatives ∇f,

iii) contains at most the square of the time derivative $\partial_0 f$ and

iv) contains no higher derivatives,

it is called *Lagrangian density* and can be written

$$\mathcal{L} \equiv \mathcal{L}(f, \partial f) \quad \text{and} \tag{2.1}$$

$$= \tfrac{1}{2}\partial_0 f \partial^0 f A(f, \nabla f) - B(f)C(\nabla f) - U(f), \tag{2.2}$$

where $C(0) = 0$. For a Lagrangian density, there is an associated integral

$$S[f] \equiv \int_{t_1}^{t_2} \int_{\mathcal{P}} \mathcal{L}(f, \partial f) \mathrm{d}^D x \mathrm{d}t, \tag{2.3}$$

which called the *action integral*, or simply *action*.

For the investigation of static topological solitons, the notion of static energy density proves very useful. The energy density can be derived as follows. First define a quantity called momentum density,

$$\Pi \equiv \frac{\partial \mathcal{L}}{\partial \partial_0 f} \tag{2.4}$$

and then define the *Hamiltonian density* by a Legendre transform,

$$\mathcal{H} \equiv \Pi \partial_0 f - \mathcal{L} \tag{2.5}$$

and if the metric is $(+ - - -)$ one can write

$$\mathcal{H} = \tfrac{1}{2}(\Pi)^2 A(f, \nabla f) + B(f)C(\nabla f) + U(f). \tag{2.6}$$

As in point particle mechanics, the Hamiltonian is related to the energy of the system and we can define

Definition 2.2 (Energy density)**.** If $\Pi = 0$, the (static) quantity

$$\mathcal{E} \equiv \mathcal{H} = B(f)C(\nabla f) + U(f) \tag{2.7}$$

is called the static *energy density* and its space-integral the static *energy*.

Since all energies in this work are static, the qualifier is usually dropped without fear of confusion.

The guiding principle in classical field theory is the so-called principle of stationary action. The principle was apparently originally suggested by Pierre Louis Maupertuis (this has been disputed) and was formulated in its current form by William Rowan Hamilton. Mathematically, it is the requirement that the action integral (2.3) is stationary under small variations of the field f with $f(t_1)$ and $f(t_2)$ fixed. From the calculus of variations, the following result is known.

Theorem 2.3 (Euler-Lagrange)**.** *The action*

$$S = \int_{t_1}^{t_2} \int_{\mathcal{P}} \mathcal{L} d^D x \, dt \tag{2.8}$$

is stationary iff

$$\partial_\mu \frac{\partial \mathcal{L}}{\partial(\partial_\mu f)} - \frac{\partial \mathcal{L}}{\partial f} = 0. \tag{2.9}$$

Proof. See, for example [35, p. 78]. □

This is the *Euler-Lagrange equation* for the Lagrangian density $\mathcal{L}$. Solutions of the Euler-Lagrange equations are interpreted as the physical entities of the theory. For the static solutions considered here, once the Euler-Lagrange equations are obtained, the time derivatives of the field(s) are assumed to be zero. Solutions are then obtained for the simplified Euler-Lagrange equations. These solutions are also solutions of the full equations.

Note that adding a constant to $\mathcal{E}$ or $\mathcal{L}$ does not alter the corresponding Euler-Lagrange equations. For sake of simplicity, it is assumed here that this addition is always done so that the global minimum of the energy is zero. The set of solutions for which $\mathcal{E} = 0$ is important enough to warrant the following definition.

Definition 2.4 (Vacuum)**.** Let f be the field and $\mathcal{L}$ the Lagrangian density of the model, $\mathcal{E}$ the corresponding energy density and the total energy $E[f] = \int_{\mathcal{P}} \mathrm{d}^D \mathcal{E} \geq 0$. The set of constant solutions of the Euler-Lagrange

equations for which $E[f] = 0$ is called the *vacuum* and is denoted

$$\mathcal{V} \equiv \Big\{ f | \partial_\mu f = 0, U(f) = 0 \text{ and } E[f] = 0 \Big\}. \tag{2.10}$$

Now consider the static case where the $\mathcal{P} = \mathbb{R}^{D+1}$ and the set $\mathcal{U} = \{f | U(f) = 0\}$ is discrete and the energy finite and therefore the boundary value $f(\infty) \in \mathcal{U}$. The discreteness of $\mathcal{U}$ means that it is not possible to alter these boundary values without costing an infinite amount of energy or altering the field discontinuously. Therefore, the boundary values must, once chosen, remain fixed. It will be demonstrated in Chapter 3 how such a situation is mathematically described in terms of homotopy classes.

The concepts defined above can be generalised to multiple fields f_j in a straightforward manner: replacing $f \to f_j$, one obtains Euler-Lagrange equations for each field from a single Lagrangian density. If the Lagrangian density does not contain any terms which depend on two different f_j, the fields decouple and can be treated independently.

In principle, it is now possible to take any Lagrangian density, write the Euler-Lagrange equations and solve them to obtain a description of the behaviour of the corresponding physical system. Unfortunately, explicitly solving the equations is only possible in very few cases. Nevertheless, important information about the system can be obtained without solving the equations, e.g. from conservation laws of the system and how they are related to the symmetries of the Lagrangian density. This is the famous Noether's theorem, which states that for each differentiable symmetry of the Lagrangian density there is a corresponding conserved current, the Noether current; and the space-integral of the 0-component of such a current is a conserved charge, the Noether charge. While these are quite important in field theory, they are not required in this investigation of topological solitons; there are continuous symmetries and the Noether currents exist, but they are not studied here.

There is another property that can be obtained from the Lagrangian density without solving the Euler-Lagrange equations, which is very important in the study of topological solitons. This is called Derrick's theorem.

2.2 Derrick's theorem

One of the most important early results regarding topological solitons is called *Derrick's theorem* [36]; it is not limited to topological solitons, but applies to stable, static, finite-energy solutions of field theories in general. The original work of Derrick considered the case where the energy density is $(\frac{\partial f}{\partial x})^2 + f(x)$; this is too limited in the present situation. Therefore, a slightly more general form of the theorem is presented. During this section, the following notation will be used: $\Phi_\lambda \equiv \Phi(\lambda x)$ and $E_\lambda \equiv E(\phi_\lambda)$.

Definition 2.5 (Localised solution)**.** A solution of the static Euler-Lagrange equations, whose energy is finite and either the energy density is or the fields themselves are asymptotically constant outside some finite region of $\mathcal{P}$, is called a *localised solution*.

Definition 2.6 (Stable solution)**.** Any solution $\Phi(x)$ of the static Euler-Lagrange equations of a field theory for which

$$\frac{\mathrm{d}}{\mathrm{d}\lambda} E_\lambda \Big|_{\lambda=1} = 0 \qquad \text{and} \qquad \frac{\mathrm{d}^2}{\mathrm{d}\lambda^2} E_\lambda \Big|_{\lambda=1} > 0,$$

will be called a *stable solution* (of the static Euler-Lagrange equations in question).

Note that this definition only concerns stability under scaling by λ. There are also other deformations and definitions of stability.

Theorem 2.7 (Derrick's theorem)**.** *Let ϕ_a be the scalar fields and $\mathcal{L}$ the Lagrangian density and of the model in question. Let the energy density of the model $\mathcal{E} = \mathcal{E}_2 + \mathcal{E}_4 + \mathcal{E}_0$ where*

$$\mathcal{E}_0 = g(\Phi), \tag{2.11}$$

$$\mathcal{E}_2 = \|\partial_j \Phi\|^2 \quad \textit{and} \tag{2.12}$$

$$\mathcal{E}_4 = f(\Phi)\partial_j\phi^a\partial_k\phi^b\partial_l\phi^c\partial_m\phi^d M^{jklm}_{abcd}(\Phi). \tag{2.13}$$

Here g and M are such smooth maps $\mathcal{P} \to \mathcal{C}$ that the corresponding integrals E_2, E_4, E_0 are finite and positive. Then the full Lagrangian density does not have stable, static, localised solutions if

$$(2-D)E_2 + (4-D)E_4 - DE_0 \neq 0 \tag{2.14}$$

or

$$(2-D)(1-D)E_2 + (4-D)(3-D)E_4 + D(D+1)E_0 \leq 0. \tag{2.15}$$

Proof. Let $\lambda > 0$. Assume that Φ is a static, localised solution of the Euler-Lagrange equations of $\mathcal{L}$. Now $E = E(\Phi) = \int \mathrm{d}^D x \big(\mathcal{E}_2 + \mathcal{E}_4 + \mathcal{E}_0\big) < \infty$ due to locality of Φ.

Now perform a uniform scaling of the solution Φ so that $\Phi \to \Phi_\lambda$ and

$$E \to E_\lambda = \int \mathrm{d}^D x \Big(\|\partial_j \Phi_\lambda\|^2 + \partial_j \phi^a_\lambda \partial_k \phi^b_\lambda \partial_l \phi^c_\lambda \partial_m \phi^d_\lambda M^{jklm}_{abcd}\big(\Phi_\lambda\big) + g\big(\Phi_\lambda\big)\Big). \tag{2.16}$$

After a change of integration variables from x to $y = \lambda x$ we obtain

$$E_\lambda = \lambda^{2-D} E_2 + \lambda^{4-D} E_4 + \lambda^{0-D} E_0, \tag{2.17}$$

This is a (possibly local) minimum under variation of λ iff

$$\Big(\frac{\mathrm{d}}{\mathrm{d}\lambda} E_\lambda\Big)\Big|_{\lambda=1} = (2-D)E_2 + (4-D)E_4 - DE_0 = 0, \tag{2.18a}$$

$$\Big(\frac{\mathrm{d}^2}{\mathrm{d}\lambda^2} E_\lambda\Big)\Big|_{\lambda=1} = (2-D)(1-D)E_2 + (4-D)(3-D)E_4 + D(D+1)E_0 > 0. \tag{2.18b}$$

Since Φ is a solution, this completes the proof. □

Note that the equation (2.18) has simpler forms, if $D \in \{1, 2, 3, 4\}$. This work deals with three dimensional theories, in which case the simplification leads to elimination of E_4 term in (2.18b).

Corollary 2.8 (Virial theorem)**.** *For any stable, localised solution of the Euler-Lagrange equations, the equation* (2.18a) *is satisfied. This is called the* virial theorem*.*

There is a similar theorem for other than scalar fields, as well. In this work, the only other kind of field present will be the gauge field. The gauge field A has to scale as $A_\lambda = \lambda A(\lambda x)$; this will be clear from the definition of the covariant derivative: the gauge field must scale like a derivative. Therefore, one can expand the definitions of $\mathcal{E}_2$ and $\mathcal{E}_4$ in Derrick's theorem

to include quadratic and quartic gauge fields, respectively, and the theorem remains unchanged otherwise.

It is worth reminding that the Euler-Lagrange equations of the energy functional do not necessarily provide a minimum of the energy, only an extremal. While it is easy to construct a theory so that the energy is bounded from below (as is always the case in this work) but not above, thus ruling out the possibility of a global maximum, the possibility of saddle points still remains. Also, the possibility of local maxima remains. These, however, can be dealt with in various ways. In the definition 2.6, the inequality is used for precisely this purpose: it ensures that any stable solution is a minimum. The possibility of a local minimum instead of global, however, remains. Indeed, this is desired and shall become evident when solutions of different homotopy classes are introduced: the solutions which are not homotopic with the vacuum will not usually be global minima of the theory, but rather global minima within their homotopy classes. Sometimes one can find solutions that are not global minima even in their homotopy classes, but are just local minima even there. The vacuum will be identified with the minimum of the homotopy class of the constant map (the trivial homotopy).

It is immediately clear from the proof of theorem 2.7 that for any Lagrangian field theory with positive definite components $\mathcal{E}_j$ of energy, the virial theorem holds for any static, stable, localised solutions. This will provide a useful check of the quality of the numerical solutions.

Due to its nature of being a proof of non-existence, a field theory which "passes" Derrick's theorem, is still not guaranteed to have static, stable, localised solutions. In fact, counterexamples can easily be found.

Next, two simple examples of field theories with topological solitons are presented.

2.3 Two simple examples

Consider a simple classical field theory with a single field $\phi : \mathbb{R}^2 \to \mathbb{R}$ and the Lagrangian density

$$\mathcal{L} = \tfrac{1}{2}\partial^\mu\phi\partial_\mu\phi - U(\phi) \tag{2.19}$$

$$U(\phi) \geq 0 \quad \forall\phi. \tag{2.20}$$

For topological solitons, the part of the Lagrangian density with time-derivatives is uninteresting, because the solitons will be static. Therefore, just the energy density is considered from now on and the notation shortened to $x = x_1$ for the rest of this section. The energy density of the theory is

$$\mathcal{E} = \tfrac{1}{2} \left|\partial_1 \phi\right|^2 + U(\phi) \tag{2.21}$$

For physical theories, the energy is (usually) required to be finite, so it is necessary that $\phi(x)$ approaches the vacuum sufficiently fast as $|x| \to \infty$. It is customary to denote $\lim_{x\to\pm\infty} \phi(x) = \phi_\pm$. It is immediately clear that here $\mathcal{V} = \{\phi | U(\phi) = 0\}$. However, there is no reason that $\phi_+ = \phi_-$. Indeed, if $\phi_+ \neq \phi_-$, an interesting situation arises: no such solution can be continuously deformed into a vacuum solution and the solutions can be classified topologically by homotopy classes.

The next question to answer is, whether the model (2.19) can evade Derrick's non-existence theorem 2.7. By substituting the values $D = 1$ and $E_4 = 0$, one sees that the conditions of possible existence of topological solitons become

$$\int_{\mathbb{R}} \tfrac{1}{2} \left|\partial_1 \phi\right|^2 \mathrm{d}x = \int_{\mathbb{R}} U(\phi) \mathrm{d}x \quad \text{, and} \tag{2.22}$$

$$\int_{\mathbb{R}} U(\phi) > 0. \tag{2.23}$$

The latter equation is easily satisfied, but whether the first equation is satisfied or not, depends, in principle, on whether the Euler-Lagrange equations allow such solutions.

Now, there is an observation by Bogomolny [37] that the above virial theorem can be manipulated so that it becomes (assuming E_0 and E_2 are finite)

$$E = \int_{\mathbb{R}} \tfrac{1}{2} \left|\partial_1 \phi\right|^2 + U(\phi) \mathrm{d}x \geq \pm \int_{\mathbb{R}} \sqrt{2U(\phi)} \partial_1 \phi \mathrm{d}x, \tag{2.24}$$

and therefore

$$E \geq \left| \int_{\mathbb{R}} \sqrt{2U(\phi)} \partial_1 \phi \mathrm{d}x \right| = \left| \int_{\phi_-}^{\phi_+} \sqrt{2U(\phi)} \mathrm{d}\phi \right|. \tag{2.25}$$

Because $U(\phi) \geq 0$, it is possible to define $\tilde{U}(\phi)$ such that $U(\phi) = \frac{1}{2}\left(\frac{\partial \tilde{U}(\phi)}{\partial \phi}\right)^2$ and therefore obtain

$$E \geq \left|\tilde{U}(\phi_+) - \tilde{U}(\phi_-)\right|, \tag{2.26}$$

and hence conclude that the (static) energy of the solution depends solely on the boundary conditions $\phi_\pm$. Energy bounds of this type, where the energy is constrained by the boundary values, are called Bogomolny bounds. Bogomolny bounds exist for many field theories. Sometimes it is also useful in solving the Euler-Lagrange equations, as shall be seen in the next section.

Note that all this has been derived without using the Euler-Lagrange equations or even the explicit form of the potential U, although its non-negativeness was required.

2.3.1 The Klein-Gordon model

Next, the specific case of the Klein-Gordon model, also called the ϕ^4 theory, is considered. In this case, the potential $U(\phi)$ is defined as follows.

$$U(\phi) = \tfrac{1}{4}\lambda(1-\phi^2)^2 = \tfrac{1}{4}\lambda(1 - 2\phi^2 + \phi^4), \tag{2.27}$$

where $\lambda > 0$.

The boundary conditions expressed in the Bogomolny bounds capture the homotopy of the field ϕ. The vacuum is now the set of two numbers $\mathcal{V} = \{-1, +1\}$ and therefore $\phi_+ - \phi_-$ is necessarily an integer, which can be normed to give the following definition:

$$N \equiv \tfrac{1}{2}(\phi_+ - \phi_-). \tag{2.28}$$

The value of N characterises the system: as soon as the boundary values are fixed, N cannot change and in a certain sense this characterisation is complete. For now, it is easy to see that $N \in \{-1, 0, +1\}$, depending on the boundary conditions. If $N = 0$, the boundary conditions are equal, the trivial solution $\phi(x) = \text{constant} = \lim_{x\to\infty}\phi(x)$ is valid and there are no interesting static solutions. If, however, $|N| = 1$, there will be a topological soliton in the system. In this simple example, it will even be possible to obtain an analytic form for it. Before that, it is worth noting that the Bogomolny bound (2.25) really is a topological one because it can be related

to N by

$$E \geq \sqrt{\tfrac{1}{2}\lambda}\left|\int_{\phi_-}^{\phi_+}(1-\phi^2)\mathrm{d}\phi\right| = \sqrt{\tfrac{1}{2}\lambda}\left|\left[\phi - \tfrac{1}{3}\phi^3\right]_{\phi_-}^{\phi_+}\right| \tag{2.29}$$

$$= \tfrac{2}{3}\sqrt{\tfrac{1}{2}\lambda}\,|\phi_+ - \phi_-| = \tfrac{4}{3}\sqrt{\tfrac{1}{2}\lambda}\,|N|\,. \tag{2.30}$$

The static Euler-Lagrange equations are now

$$\partial_1\partial_1\phi + \lambda\phi(1-\phi^2) = 0. \tag{2.31}$$

In principle, this equation could be solved as is, but this particular theory has an easier equation to solve, as well. In the derivation of the Bogomolny bound, a simple inequality is necessary:

$$\left(\frac{1}{\sqrt{2}}\partial_1\phi \pm \sqrt{U(\phi)}\right)^2 \geq 0. \tag{2.32}$$

A field is said to *saturate* the Bogomolny bound if the equality above holds. This can then be solved easily to obtain

$$\phi = \tanh\left((x+a)\sqrt{\tfrac{1}{2}\lambda}\right). \tag{2.33}$$

This is also a solution of the Euler-Lagrange equation (2.31) as can easily be checked. The energy density (2.21) becomes

$$\mathcal{E} = \tfrac{\lambda}{2}\operatorname{sech}^4\left(\sqrt{\tfrac{1}{2}\lambda}(x+a)\right). \tag{2.34}$$

Solutions of this type, which interpolate between two different (fixed) boundary values, are called kinks; as can be seen in Fig. 2.1a, the name is well deserved and descriptive. The shape of the energy density has a well defined peak at $x = -a$, so this can reasonably be called the location of the soliton and the requirements of definition 2.5 are clearly met.

2.3.2 The sine-Gordon model

The sine-Gordon theory is obtained from (2.19) by specifying the following potential

$$U(\phi) = (1 - \cos\phi). \tag{2.35}$$

It is immediately clear that $U(\phi) = 0 \Leftrightarrow \phi \in 2\pi\mathbb{Z}$ and therefore $\mathcal{V}$ is isomorphic to $\mathbb{Z}$ and, as in the case of the Klein-Gordon model, the boundary conditions dictate the topology of the system. The boundary values are now $n \in \mathbb{Z}$ and $\phi_\pm = 2\pi n$. There is again a constant of motion defined by the unchanging boundary values, given by

$$N \equiv \tfrac{1}{2\pi}(\phi_+ - \phi_-). \tag{2.36}$$

This is clearly an integer and like in the Klein-Gordon theory, it completely characterises the system in some sense. It is not a coincidence that a similar invariant exists in both the Klein-Gordon and sine-Gordon -theories; such invariants that cannot change in continuous deformations are given a more general and detailed mathematical description in Chapter 3.

Due to the translation invariance of the theory, there is a simplification that can be made: if $m \in \mathbb{Z}$, changing $\phi \to \phi + 2\pi m$ does not change $\mathcal{L}$, so we can always choose, without loss of generality, $\phi_- = 0$.

The Euler-Lagrange equation of Eqs. (2.19) and (2.35) is

$$\partial_0\partial^0\phi = \partial_1\partial^1\phi + \sin\phi, \tag{2.37}$$

which reduces to (compare with (2.31))

$$\partial_1\partial_1\phi = \sin\phi \tag{2.38}$$

for static fields (note that the metric is $(+-)$). The static equation can be solved; the solution is

$$\phi = 4\arctan\left(\mathrm{e}^{x-a}\right), \tag{2.39}$$

where a is an integration constant (the other being fixed by the boundary conditions). The above solution also saturates the Bogomolny bound (2.24), just like the static solution of the Klein-Gordon model. Given suitable initial conditions, the dynamical equation can also be directly integrated, but one solution can also be obtained simply by giving the static solution a Lorentz boost. Because of the Lorentz invariance of (2.19), such a ϕ will automatically be a solution of the dynamical equation. One example of the static solution is displayed in Fig. 2.1b, showing how the value of ϕ starts from 0 and smoothly interpolates into 2π.

It is often useful to have an idea of the "location" of a topological soliton.

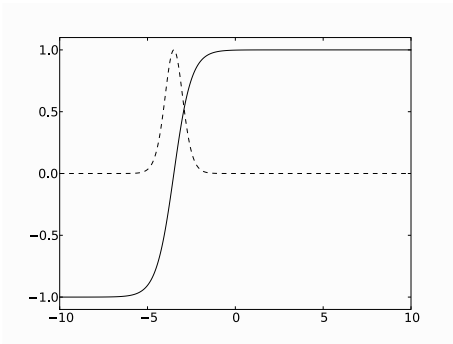

(a) A kink solution (solid curve) of the Klein-Gordon theory and its energy density (dashed curve) with $\lambda = 2, a = 3.5$.

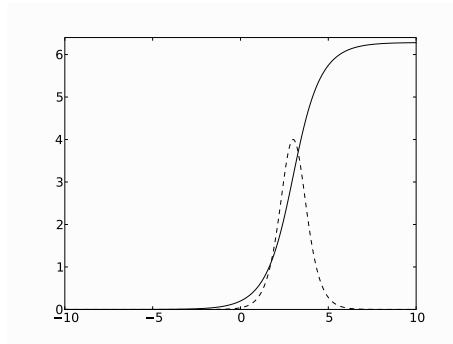

(b) The field ϕ/π (solid curve) and the energy density (dashed curve) of the sine-Gordon model with $a = 3$.

Figure 2.1: Kink solutions of the Klein-Gordon and sine-Gordon models.

However, a suitable definition for the location is not always immediately clear, as shall be seen in the case of the Faddeev-Skyrme model. In the case of the sine-Gordon theory, the energy density gives a reasonable definition for the location. The energy density (2.21) becomes $\mathcal{E} = 4\,\mathrm{sech}^2\big(x - a\big)$, which has a single maximum at $x = a$. Thus the location of the maximum can be called the location of the soliton. For a dynamical soliton, the maximum of course moves as the soliton moves. The energy density is also displayed in Fig. 2.1b.

Chapter 3

Topology

It was seen in Chapter 2, how sometimes the fixed boundary conditions prevent the solution from evolving into a vacuum configuration since it would require an infinite amount of energy or altering the field in a discontinuous way. While the latter option is allowed in quantum theories, where it becomes the tunneling effect, in classical theory, neither option is realisable and therefore these boundary conditions cannot be changed once fixed. Furthermore, they were used to characterise the system in a way which describes the whole system using only the boundary conditions, c.f. (2.28). The characterisation of a field configuration by such invariant properties is quite common in physics. In principle, any conserved quantity can be so used to characterise a system, but the N of (2.28) belongs to a rather special class of conserved quantities, called *topological invariants*. In order to give a definition of topological invariants in general, some concepts and results from topology are presented in this Chapter, providing the foundation for the application of topology to classical field theory. The main player will be a property called *homotopy*, which describes how two maps (such as two different field configurations) can (or cannot) be continuously deformed into each other. In the context of physics, this deformation is often interpreted as the time evolution of the system. Hence, if the field configurations cannot be continuously deformed into each other, they are in some sense decidedly different, whereas if they can they are in some sense equal. The approach here will be rather heuristic, without explicit proofs of the various theorems; pointers to suitable references for the proofs are given after the theorems.

Next, to lay the foundation of the term topological soliton, some ideas from algebraic topology are quoted.

3.1 Topology of space

While this work is not concerned with the topology of physical space, $\mathcal{P}$, it is worth clarifying what is meant by its topology. Currently, there are no observations which (clearly) indicate that the space would be topologically non-trivial, but it is very difficult to rule it out either. Non-trivial topology of physical space includes some closed, like toroidal, universes and various other features, like wormholes, which can be realised as solutions of the Einstein field equations of the general theory of relativity; in topological terms these features make the space multiply connected.

3.2 Topology in field theories

Topological features in field theories refer to the properties of the fields. The set of possible field configurations are classified according to their topological properties. The classification depends on both the physical and configuration spaces, but the topological properties of the spaces themselves are not analysed. Here only the topology of scalar fields is considered and the theories are divided in two. The first set contains theories where the field takes values on $\mathbb{R}$ or $\mathbb{R}^n$ if there are n fields. The second set contains theories where the fields take values on a subset of $\mathbb{R}^n$ defined by a non-linear constraint equation, for example the static field can be a map $f : \mathbb{R}^D \to \mathbb{R}^n$ with a constraint $\|f\| = 1$.

It will be seen that if the n fields take values on $\mathbb{R}^n$, the topological properties arise from the symmetries of the vacuum $\mathcal{V} \subset \mathcal{C}$. It will be necessary that $\mathcal{V} \subsetneq \mathcal{C}$ and that $\operatorname{card} \mathcal{V} > 1$, otherwise the topological properties are trivial. The situation is slightly different if the fields take their values on a subset of $\mathbb{R}^n$. In this case, the properties of the vacuum manifold are not important; indeed even the case $\mathcal{V} = \mathcal{C}$ may now yield interesting topology, as will be seen in the context of the Faddeev-Skyrme model.

The classification the fields $f : \mathcal{P} \to \mathcal{C}$ according to their topological properties is accomplished by dividing the fields into *homotopy classes*. This is important because members of one homotopy class cannot be transformed into members of another class with continuous transformations (homotopies), such as the usual time-evolution. Therefore, if there are multiple classes, there can be field configurations which are in some sense different. Mathematically, the difference is encoded into a *homotopy invariant*. These concepts will be introduced in Section 3.3.

It should be noted, that it is not *a priori* clear, whether there is more than one homotopy class. If there is only one class, all fields can be deformed into the vacuum configuration and the model is topologically trivial. Also, even if there are multiple homotopy classes, it is not guaranteed that static, localised solutions of the field equations are found in all classes. For example, in the static sine-Gordon theory, it can be shown that there are no static, localised solutions of the field equations for $N > 1$ [38, p. 117].

If there are more than one homotopy class with solutions of the field equations, such solutions are called topological defects or topological solitons, depending on context. In this work, such solutions are desired features of the system and therefore called topological solitons. A more thorough definition of a topological soliton will be given in Section 3.4.

The process by which the vacuum manifold causes the topological properties of the field f is called the Kibble [13] or Kibble-Zurek [13, 39] mechanism and will be detailed in Section 3.3. The fact that homotopies cannot change some properties of a field and that the usual time-evolution is continuous (a homotopy), means that something different is required to produce (or destroy) topological solitons. One example is a phase transition. It is possible for the vacuum structure of the model to change in a phase transition, therefore allowing topological solitons to form (or disappear).

3.3 Homotopy

The definitions of algebraic topology presented here are not necessarily the most general forms possible, but in order to avoid unnecessary mathematical detail, they are formulated so that they are sufficient for this work. A more mathematical discussion of the matter can be found in books [40] and [41].

Definition 3.1 (Homotopy)**.** Let f and g be smooth maps $X \to Y$ and $I = [0, 1]$, the unit interval. If there exists a smooth map $h : X \times I \to Y$ such that $\forall x \in X : h(x, 0) = f(x)$ and $h(x, 1) = g(x)$, h is called *homotopy* between f and g, and it is said that f and g are *homotopic*. We denote this by writing $f \simeq g$.

Note. A common notation for homotopy is $h_t(x) = h(x, t)$, where the homotopy condition becomes $h_0 = f, h_1 = g$.

The fact that two maps f and g are homotopic means that they can be continuously deformed into each other, like the famous coffee mug and

doughnut. In physics the interval I is usually time and h_t therefore becomes the time evolution of a field configuration f into g. Time evolution is usually considered smooth and therefore all the future field configurations that f evolves to are homotopic to f. So, if there are two non-homotopic field configurations, they will stay non-homotopic. This is the basic building block of a topological soliton: the fact that two non-homotopic field configurations will stay non-homotopic and two homotopic ones will stay homotopic provides us with a reason to use the term topological soliton. The qualifier "topological" is used to distinguish the concept from the usual meaning of the term soliton because a topological soliton is not necessarily a soliton in the usual sense.

It is easy to see that homotopy is an equivalence relation: it is symmetric because the time interval can be reversed, it is transitive because the unit interval can be joined and scaled, and it is reflexive because f is trivially homotopic to itself. Thus maps $X \to Y$ can be classified into equivalence classes. Sometimes there is just one equivalence class, the class of maps homotopic to the constant map $c : X \to Y,\ c(x) = c$. This is the case, for example, if $Y = \mathbb{R}$, because for any X and $f : X \to Y$, one can set $h(x,t) = (1-t)f(x) + tc$. The same works for all $\mathbb{R}^n$, which may, at first look, put this whole consideration of homotopies into a slightly odd light: what is its role in such a theory, where the configuration space is $\mathbb{R}^n$ (or $\mathbb{C}^n$) and topology is trivial there? This will become evident in a moment, but first the theory of homotopies is developed a little further. To accomplish this, the concept of based homotopy is defined and a restriction placed on X.

Definition 3.2 (Based homotopy)**.** A homotopy h_t between maps $f, g : X \to Y$ for which there exists a y_0 for which $\forall t : h_t(\partial X) = f(\partial X) = y_0$, is called a *based homotopy.*

Now consider based maps when $X = \mathbb{R}^D$. The requirement that boundary of X maps to a single point in Y means that one can perform the *one-point compactification* of X by identifying topologically $\mathbb{R}^D \cup \{\infty\} = \mathsf{S}^D$, the D dimensional sphere, i.e. surface consisting of the points of the set $\{x \in \mathbb{R}^{D+1} \big| \|x\| = 1\}$. Next, consider S^1, where continuity demands $f(0) = f(2\pi) = f(\infty)$, therefore making the image $f(\mathsf{S}^1)$ a closed path. Such a map is called a *loop.* For $D > 1$ the analog is a map where a single point, call it p, on the S^D takes the role of the point at infinity (in $\mathbb{R}^D$) and continuity demands that $f(p) = \lim_{\|x\to\infty\|} f(x)$. For loops and their higher

dimensional analogs, it is possible [41, p. 340] to define an operation called *composition*, which provides the set of equivalence classes of maps $\mathsf{S}^D \to Y$ with group structure. The composition itself is not needed in this work, so the details are not presented here; they can be found in [41, p. 340]. The fact that this becomes a group, however, is very important because it ensures that compositions of maps stay within the same homotopy class and allows one to discuss isomorphisms between homotopy groups and some more familiar groups.

Definition 3.3. The group of equivalence classes of maps $\mathsf{S}^D \to Y$ is called the *Dth homotopy group of Y* and denoted $\pi_D(Y)$.

The concept of homotopy group is very powerful. For example, the simply connectedness of a set can easily be checked if its first homotopy group is known: it is a theorem that any connected set is simply connected iff its first homotopy group (i.e. π_1) is trivial (i.e. the group of one element). Other very powerful results also follow, although the computation of the homotopy groups themselves is sometimes highly non-trivial. In this work, it is assumed that the field f is either a single scalar field or a multiplet of scalar fields. Sometimes, the scalars are coupled to gauge fields, but other than that, there are no other fields and the topology of gauge fields is not discussed.

If fields are continuous maps to $\mathbb{R}^n$, their topology becomes trivial, as noted above, and there are no topological solitons. However, if some restrictions are placed on the fields, a different picture emerges. In field theory, the domain of the static fields is usually $\mathbb{R}^D$. Physical arguments often lead to considering fields whose energy density falls rapidly to zero when $r \to \infty$, where r is the distance from the origin. It also makes sure that whenever $r \to \infty$, the field $f \in \mathcal{V}$, providing a boundary condition. This is crucial, because now the possibility of something with non-trivial topology exists! Another usual physical argument is the finiteness of the energy of the system, but the previous argument is sufficient, for now. The decay of energy density may not be rapid enough to guarantee a finite energy, but it does provide a system with localised solutions according to definition 2.5. Now, if there is non-trivial topology, there is also automatically a localised solution, so there finally is something that can reasonably be called a (still undefined) topological soliton.

The non-trivial topology arising from the properties of the vacuum and the ensuing boundary condition $\lim_{r\to\infty} f(r) \in \mathcal{V}$ is due to the fact that

topologically, no information is lost if only the boundary $\partial\mathbb{R}^D = \mathsf{S}^{D-1}$ is considered instead of the whole $\mathbb{R}^D$. Now the field configuration on the boundary becomes a map $f : \mathsf{S}^{D-1} \to \mathcal{V}$, which is non-trivial whenever $\pi_{D-1}(\mathcal{V}) \neq 0$. For a vast class of field theories, this is indeed the case. Note that if $\mathcal{V} = \mathcal{C}$, the triviality of $\mathcal{C}$ is carried over to the vacuum and there are no topologically non-trivial maps. This also happens if the vacuum is a single point: then all maps $\mathsf{S}^{D-1} \to \mathcal{V}$ necessarily are homotopic. Such cases are therefore excluded from the following considerations.

Fields with non-trivial topology at the boundary will usually have divergent energy, regardless of how fast $\lim_{r\to\infty} f(r) \in \mathcal{V}$, because there will be gradients of f in the Lagrangian and they will not vanish. This is easy to see when considering a $D+1$-dimensional model with a Lagrangian containing a term like $\partial_\mu f \partial^\mu f$ and writing the static energy in polar coordinates. If $f(\infty) \in \mathcal{V}$, the integral of the gradient term in the angular direction can be performed and is finite, leaving a radial integral $\int^\infty r^{D-3}\mathrm{d}r$, which is divergent for $D > 1$. Finite energy systems can be constructed by coupling the field(s) to a gauge field. The gradient term is now replaced by covariant derivatives, which it is sometimes possible to arrange the covariant derivative to vanish so fast that the energy remains finite, but it is not always the case.

The case of constrained fields is different: now, the energy is required to be finite. It follows from a similar argument regarding the gradient terms in the energy functional as in the first case, that energy can only be finite in an infinite space, if $\exists c \in \mathcal{C} : \lim_{r\to\infty} f(r) = c \in \mathcal{V}$. Topologically, this requirement is equivalent to the one-point compactification of $\mathbb{R}^D$ used earlier. Thus, the homotopy group considered in the this case is $\pi_D(\mathcal{C})$. Note that, if there is a potential, it imposes the restriction that c must be such that $c \in \mathcal{V}$ in order to keep the energy finite. The existence of a potential is generally not required now, unlike in the case of unconstrained fields, because the topology of $\mathcal{C}$ itself may be non-trivial. These fields can also be coupled to gauge fields, which can alter the requirement of finite energy just like for unconstrained fields. This expands the possibilities greatly such cases and are not considered in this work.

The exact form of the Lagrangian of the field theory has intentionally been left unspecified. The details of the Lagrangian may complicate the topological features of the system, as was seen with the coupling of fields to gauge fields.

This digress into homotopy theory is now ready to be finished by defin-

ing one last concept.

Definition 3.4 (Topological invariant)**.** Let $\mathcal{P}$ and $\mathcal{C}$ be topological spaces and $f : \mathcal{P} \to \mathcal{C}$ a smooth map. Any property of f which is unchanged under homotopy, is called a *topological invariant* or *homotopy invariant*.

The topological invariant used most often is the homotopy class of f; in this case f is identified with its equivalence class as an element of the homotopy group of maps $\mathcal{P} \to \mathcal{C}$.

3.4 Topological soliton

The word *soliton* has different meanings, depending on the context. These include the classical solitons: localised, smooth solutions of completely integrable systems that scatter elastically, experiencing just a phase shift, and do not change shape with time. These features are consequences of the complete integrability of the system, and while the objects studied in this work share some of these characteristics, they are not (known to be) completely integrable - except the example in Section 2.3.2. Therefore, it is desirable to distinguish the solitons considered in this work from solitons of integrable systems; the concept of *topological soliton* is used for this purpose.

Definition 3.5 (Topological soliton)**.** Let $\mathcal{L}(f, \partial f)$ be a Lagrangian of some field theory, where $f : \mathcal{P} \to \mathcal{C}$ is a smooth map. A solution $\tilde{f}$ of the static Euler-Lagrange equations of $\mathcal{L}$ is called a *topological soliton* iff

$$\tilde{f} \text{ is stable (definition 2.6)} \tag{3.1}$$

$$\tilde{f} \text{ is localised (definition 2.5), and} \tag{3.2}$$

$$\tilde{f} \text{ possesses a non-trivial topological invariant (definition 3.4).} \tag{3.3}$$

Topological solitons can also be defined for dynamical solutions instead of just static ones, but those are outside the scope of this work. Since time evolution is considered as the homotopy, the topological properties of a topological soliton are preserved even in a dynamical theory. Similarly, the locality and stability against scaling (although the definitions for these are not necessarily usable any more) are also preserved. There are also dynamical topological solitons that are not constructed from static ones.

Some of these do not move at all, but oscillate instead, like some breather solutions of the sine-Gordon model [42].

3.5 On homotopy classifications

In this section, methods to classify topological solitons by their homotopies will be developed. Computing the homotopy groups π_D of a space is highly non-trivial, except in some rare cases. One example of the easy cases was seen above, where the homotopic equivalence classes of $\mathbb{R}$ were considered. Considering a based map does not alter the situation in this case at all: the same homotopy still works for all maps, thus proving that $\forall n, m \in \mathbb{N}$: $\pi_n(\mathbb{R}^m) = 0$. The non-trivial situations require more work and the proofs would require such a long detour into algebraic topology, homology and differential geometry that they will be given here as references only.

3.5.1 Homotopy groups of spheres

Theorem 3.6. *Let $m, n \in \mathbb{N}$. For all $m < n$,*

$$\pi_m(\mathsf{S}^n) = 0. \tag{3.4}$$

Proof. The quite simple proof can be found in [41, p. 349]. □

Theorem 3.7. *Let $n \in \mathbb{N}$. The nth homotopy group of n-sphere is isomorphic to the group of integers,*

$$\pi_n(\mathsf{S}^n) = \mathbb{Z}. \tag{3.5}$$

Proof. See [41, p. 361]. □

It is easy to construct a map homotopic to a member of a chosen equivalence class of $\pi_n(\mathsf{S}^n)$. Before doing that, however, it is helpful to introduce a method to directly determine the class of a given map.

Definition 3.8 (Degree)**.** Let $f : X \to Y$ be a proper map, f^* its pullback, $\dim X = \dim Y$ and ω a normalised volume form on Y. The value of

$$\deg f \equiv \int_X f^*\omega \tag{3.6}$$

is called the *degree of* f.

For spheres, it is now easy to construct a member of any homotopy class. Consider the function $f : \mathsf{S}^n \to \mathsf{S}^n$ for which $f(x) = (r\cos k\phi, r\sin k\phi, x_2, \ldots, x_n)$, where $k \in \mathbb{Z}$ and x_i are the natural coordinates of $\mathbb{R}^{n+1}$ in which the S^n is embedded. Let ω be the unit volume form of S^n, $A(n)$ the area of S^n and $V(n)$ the volume of n-ball D^n. Now,

$$\begin{aligned}\deg f &= \int_{\mathsf{S}^3} f^*\omega \\ &= \frac{1}{A(n)}\frac{1}{n!}\int_{\mathsf{S}^n} \epsilon^{i_0 i_1 \ldots i_n} f_{i_0} \bigwedge_{k=1}^{n} \mathrm{d}f_{i_k} \\ &= \frac{1}{A(n)}\int_{\mathsf{S}^n} \Big(\sum_{j=0}^{n} f_j \bigwedge_{k=1,k\neq j}^{n} \mathrm{d}f_k\Big).\end{aligned}$$

Using polar coordinates $x_0 = \cos\theta$ and $x_1 = \sin\theta$, one finds that $\mathrm{d}f_0 = -k\sin(k\theta)\mathrm{d}\theta$, $\mathrm{d}f_1 = k\cos(k\theta)\mathrm{d}\theta$ and $\mathrm{d}f_0\mathrm{d}f_1 \propto \mathrm{d}\theta \wedge \mathrm{d}\theta = 0$. Thus

$$\begin{aligned}\deg f &= \frac{1}{A(n)}\int_{\mathsf{D}^{n-1}} \prod_{j=2}^{n} \mathrm{d}x^j \int_0^{2\pi} k\mathrm{d}\theta \\ &= \frac{1}{A(n)} V(n-1)2\pi k \\ &= k,\end{aligned}$$

by using the relation $2\pi V(n-1) = A(n)$.

Theorem 3.9. *For a smooth map $f : X \to Y$,*

$$\deg f \in \mathbb{Z}. \tag{3.7}$$

Proof. See [40, p. 41]. □

It is now easy to note that the degree is invariant under homotopies. Because the degree is an integer, it cannot change under continuous deformations. There is a also a much stronger result.

Theorem 3.10. *The degree map* $\deg : \pi_n(\mathsf{S}^n) \to \mathbb{Z}$ *is an isomorphism.*

Proof. See [40, p. 215] for the rather complicated proof. □

The homotopy class of a map f is now equal to its degree and thus the (in principle) simple computation of the degree can be used to determine if two maps are homotopic. Also, the relative ease with which maps of any degree can be constructed will be useful later.

These results are sufficient for many purposes in physics. In the case of unconstrained static fields, the domain is usually $\mathbb{R}^D$ with $D \in \{2, 3\}$, giving the first and second homotopy groups of the vacuum manifold. It is now easy to construct a field theory where the vacuum manifold happens to be S^{D-1}, yielding a homotopy group isomorphic to the integers. For constrained fields, it is very often the case that the configuration space is a sphere, immediately yielding homotopy groups $\pi_m(\mathsf{S}^n)$, where $m \leq n$.

There are only three classes of important field theories where these theorems 3.6 and 3.7 do not suffice.

One such class is the set of field theories, where the physical space is not $\mathbb{R}^D$ nor a sphere (compactified $\mathbb{R}^D$). These shall be discussed in Section 3.5.2. The two other cases provide two important special cases. First is the special case where the domain is $\mathbb{R}$ - this is the case in the sine-Gordon model, for example. The boundary of the domain now becomes a disconnected set of two points, which is here denoted by S^0 for consistency. The classification into homotopy classes works like before, but in general they are not groups (the definition of the group operation fails). They are nevertheless denoted by $\pi_0(Y)$; its elements are maps from a single point to Y and therefore $\pi_0(Y)$ is the set of disconnected components of Y. If Y is connected, all maps are homotopic and $\pi_0(Y)$ is a group - the trivial group of a single element.

Suppose now that the domain of an unconstrained field f is $\mathbb{R}$ and the vacuum manifold is $\mathcal{V}$, yielding the boundary $\{\pm\infty\}$. Thus at both boundaries f is a member of $\pi_0(\mathcal{V})$, which is supposed to be non-trivial. Thus f can be considered as member of $\pi_0(\mathcal{V}) \times \pi_0(\mathcal{V})$. If $f(-\infty) = f(\infty)$, the field has trivial topology: $h(t, x) = tf(\infty) + (t-1)f(x)$ is the required homotopy. If $f(-\infty) \neq f(\infty)$, the field interpolates from $f(-\infty)$ to $f(\infty)$ and there is no homotopy which would take f to a constant map because the values $f(\pm\infty)$ must not change because that would require an infinite amount of energy. Thus topological invariance is guaranteed. For all models considered in this work, $\operatorname{card} \pi_0(\mathcal{V}) \leq \operatorname{card} \mathbb{Z}$ and therefore the topological invariant has an integer nature as was in Sections 2.3.1 and 2.3.2, where $\operatorname{card} \pi_0(\mathcal{V}) < \operatorname{card} \mathbb{Z}$ and $\operatorname{card} \pi_0(\mathcal{V}) = \operatorname{card} \mathbb{Z}$, respectively.

The third case is the class of field theories, where $m > n$. For other

combinations of m, n other than $(3, 2)$, the homotopy group becomes increasingly more difficult to compute (and usually also more complex), a large list of such homotopy groups can be found in [41, p. 339]. The case $m = 3, n = 2$, while not necessarily any easier to compute than the others, is one of the cases considered in this work.

Theorem 3.11. *The 3rd homotopy group of 2-sphere is isomorphic to the group of integers,*

$$\pi_3(\mathsf{S}^2) = \mathbb{Z}. \tag{3.8}$$

Proof. See [41, p. 375]. □

There is a method to compute the homotopy class a map $f : \mathsf{S}^3 \to \mathsf{S}^2$. It requires some concepts from differential geometry, that the reader is assumed to be familiar with. The definitions can be found in references [43] and, if a more rigorous treatment is desired, in [40].

Definition 3.12 (Hopf invariant)**.** Let $n \in \mathbb{N}$, $f : \mathsf{S}^{2n-1} \to \mathsf{S}^n$, f^* its pull-back, α be the unit area form of S^n, ω such that $\mathrm{d}\omega = f^*\alpha$ and $H : C^\infty(\mathsf{S}^{2n-1}, \mathsf{S}^n) \to \mathbb{R}$ a map defined by

$$H(f) = \int_{\mathsf{S}^{2n-1}} \omega \wedge \mathrm{d}\omega. \tag{3.9}$$

The value $H(f)$ is called the *Hopf invariant* of f.

It can be shown that $H(f)$ exists (the required 1-form ω always exists), is independent of the choice of α and ω and that it is indeed invariant under homotopies of f [40, p. 228]; as a consequence, the Hopf invariant is sometimes defined on $\pi_{2n-1}(\mathsf{S}^n)$ instead of $C^\infty(\mathsf{S}^{2n-1}, \mathsf{S}^n)$. This yields an equivalent definition. There are many results regarding the Hopf invariant (see [40, Chapter 17] and [41, Chapter 4.B]), the most important here being the following, which radically changes the naive domain $\mathbb{R}$ of the Hopf invariant.

Theorem 3.13. *The Hopf invariant $H : \pi_{2n-1}(\mathsf{S}^n) \to \mathbb{Z}$ is a* homomorphism *and for $n = 2$ it is an* isomorphism*.*

Proof. For the first part, see [41, Proposition 4B.1]. For the second part, recall that that $\pi_3(\mathsf{S}^2) = \mathbb{Z}$ (theorem 3.11); the result then follows from [41, Corollary 4B.2]. □

As an isomorphism, the Hopf invariant provides a useful way to classify maps $\mathsf{S}^3 \to \mathsf{S}^2$ and for the remainder of this work, the Hopf invariant shall be taken to refer only to the case $n = 2$. The Hopf invariant also provided a reason for the next definition.

Definition 3.14 (Hopfion)**.** A topological soliton which is classified by the Hopf invariant is called a *Hopfion*.

Like the degree, the Hopf invariant is also called a topological quantum number or topological charge.

There is an important property of $\pi_3(\mathsf{S}^2)$ which relates it to $\pi_3(\mathsf{S}^3)$ by something called the Hopf map.

Definition 3.15 (Hopf map)**.** Let σ_j be the Pauli matrices. Denote the cartesian coordinates of $y \in \mathsf{S}^3$ by the column vector $y = (y_1, y_2, y_3, y_4)^T$, where $\|y\| = 1$ so that $y \in \mathsf{S}^3$. Define $h : \mathsf{S}^3 \to \mathsf{S}^2$ by

$$h(y) \equiv y^\dagger \vec{\sigma} y = \begin{pmatrix} 2(y_1 y_3 + y_2 y_4) \\ 2(y_2 y_3 - y_1 y_4) \\ y_1^2 + y_2^2 - y_3^2 - y_4^2 \end{pmatrix}. \tag{3.10}$$

The map h is called the *Hopf map* and *Hopf fibration*.

It is easy to see that, if we denote $z_0 = y_1 + iy_2$ and $z_1 = y_3 + iy_4$, then $h(y) = (2\Re(z_0\overline{z_1}), 2\Im(z_0\overline{z_1}), |z_0|^2 - |z_1|^2)$, and $\|h(y)\| = 4|z_0\overline{z_1}|^2 + |z_0|^4 - 2|z_0|^2|z_1|^2 + |z_1|^4 = (|z_0|^2 + |z_1|^2)^2 = \|y\|^2 = 1$. Thus h is indeed a map to S^2.

The Hopf invariant of the Hopf map is historically quite important and we will also need the result shortly.

Theorem 3.16. *Let $h : \mathsf{S}^3 \to \mathsf{S}^2$ be the Hopf map and $H : C^\infty(\mathsf{S}^3, \mathsf{S}^2) \to \mathbb{Z}$ the map giving the Hopf invariant. Then*

$$H(h) = 1. \tag{3.11}$$

Proof. See [40, p. 235] □

The following theorem now gives us a correspondence between maps from $\mathsf{S}^3 \to \mathsf{S}^3$ and $\mathsf{S}^3 \to \mathsf{S}^2$.

Theorem 3.17. *Let $f : \mathsf{S}^3 \to \mathsf{S}^3$ be a smooth map and $h : \mathsf{S}^3 \to \mathsf{S}^2$ the Hopf map. The value of the Hopf invariant of $h \circ f$ is*

$$H(h \circ f) = \deg f. \tag{3.12}$$

Proof. Let α be the unit area form of S^2 and ω the unit volume form of S^3. The left hand side of (3.12) equals $\int \omega' \wedge \mathrm{d}\omega'$, where ω' is such that $\mathrm{d}\omega' = (h \circ f)^* \alpha$ and the right hand equals $\int f^* \omega$. Now,

$$\mathrm{d}\omega' = (h \circ f)^* \alpha = \alpha \circ h \circ f = f^*(\alpha \circ h) = f^*(h^* \alpha) = f^*(\mathrm{d}\omega) \tag{3.13}$$

$$= \mathrm{d}(f^* \omega), \tag{3.14}$$

which holds, if $h^* \alpha = \mathrm{d}\omega$. This is equivalent to the requirement that one can compute $H(h)$, which is always possible. Therefore, one may write

$$H(h \circ f) = \int_{\mathsf{S}^3} \omega' \wedge \mathrm{d}\omega' = \int_{\mathsf{S}^3} f^* \omega \wedge \mathrm{d}(f^* \omega) = \int_{\mathsf{S}^3} f^*(\omega \wedge \mathrm{d}\omega) \tag{3.15}$$

$$= \deg f, \tag{3.16}$$

where again a further result is needed to justify the last equality because it requires that $\omega \wedge \mathrm{d}\omega$ is the unit volume form. This is not a trivial requirement, but it is equivalent to the requirement that $H(h) = 1$, theorem 3.16. This completes the proof. □

The fields with topological invariants are customarily given descriptive names according to their dimension, whether they are constrained or not and their respective homotopy groups. Some of these are summarised in table 3.1.

3.5.2 Torus homotopies

When the domain of the static fields is not the compactification S^D of $\mathbb{R}^D$ nor the compactification S^{D-1} of the boundary of $\mathbb{R}^D$, the homotopy groups of spheres cannot be used to classify the field configurations.

The Abrikosov lattice [4] of two-dimensional superconductors is one such situation: mathematically, the vortices can be modelled as a gauged complex scalar field living on a 2-torus, T^2, with flat a metric (the domain is simply $\mathbb{R}^2$ with a periodicity condition imposed on the fields). Homo-

	unconstrained fields		constrained fields	
D	homotopy	descriptive name	homotopy	descriptive name
1	$\pi_0(\mathcal{V})$	Kink Domain wall	$\pi_1(\mathcal{C})$	Kink Domain wall
2	$\pi_1(\mathcal{V})$	Vortex Cosmic string	$\pi_2(\mathcal{C})$	Baby Skyrmion
3	$\pi_2(\mathcal{V})$	Monopole	$\pi_3(\mathcal{C})$	Hopfion Skyrmion

Table 3.1: Classification of static fields of dimension D with topological invariants

topy classes of maps, whose domain is a torus, are sometimes called torus homotopies, a term introduced in [44].

Two other examples are studied in [34], where the domain is either $\mathsf{S}^2 \times \mathsf{S}^1$ or T^3 and the constrained fields take values on S^2. The homotopy classification is now much more complicated than in the case of a spherical domain. Instead of a single homotopy invariant completely classifying the fields, there are now two, or four. The classification is originally due to Pontrjagin [45], but here a corollary of the restricted version of [46] is sufficient.

Theorem 3.18 (Pontrjagin)**.** *Let $f : \mathsf{S}^2 \times \mathsf{S}^1 \to \mathsf{S}^2$. There are two homotopy invariants of f: a primary invariant $s_2 \equiv \deg f\big|\mathsf{S}^2$ and if $s_2 \neq 0$ there is a secondary invariant $s_1 \in \mathbb{Z}_{2s_2}$ for each class s_2. Let $g : \mathsf{T}^3 \to \mathsf{S}^2$. There are three primary homotopy invariants of g: t_1, t_2, t_3. Denote $t = \gcd(t_1, t_2, t_3)$ to define a secondary invariant, h_t, which depends on t. If $t = 0$, $h_t = H(f)$ and if $t \neq 0$, the $h_t \in \mathbb{Z}_{2t}$ for each t.*

Proof. See Theorem 1 of [46], where a more general result is proven, whose special case this is. □

The nature of the invariants t_i require a detailed description. Consider a map $f : \mathsf{T}^3 \to \mathsf{S}^2$ and a regular value $p \in \mathsf{S}^2$. Now, the preimage $f^{-1}(p)$ is a closed path on the domain and therefore can be represented by a directed

path $\gamma : \mathsf{S}^1 \to \mathsf{T}^3$. Now, each t_i counts the number of times γ travels around the respective S^1 of the T^3, as shall be seen in 3.5.3.

Note that it is possible to change the integration domain in the definition 3.12 of the Hopf invariant. If one changes the domain to $\mathsf{S}^2 \times \mathsf{S}^1$ or T^3, the value of the integral is still here called the Hopf invariant, although it is no longer homotopy invariant except in the case $t = 0$, where $H = h_0$.

Due to the secondary invariants s_1 and h_t, the primary invariants are not sufficient for complete homotopy classification. However, two homotopic maps have the same invariants s_i or t_i, h_t, but two maps with the same s_2 or t_1, t_2, t_3 are not necessarily homotopic. The complete classification is not required to establish the existence of topological solitons and in this work, we only deal with the primary invariants t_i and s_2.

3.5.3 Determining the homotopy group of a map

It is not always easy to determine the homotopy group of a given map. The integrals involved in definitions 3.12 and 3.8 are usually too complicated to compute analytically, and numerical methods must be used. Therefore, it is desirable to have an alternative, independent method of computing the invariants. Fortunately, such a method exists for all the homotopy invariants considered in this work. These methods are described in this section.

The alternate method of computing the Hopf invariant requires the concept of linking number. The exact mathematical definition can be found in [40, p. 229-234], here a heuristic approach is used. Suppose that f is a smooth map $\mathsf{S}^3 \to \mathsf{S}^2$, choose two distinct points $y_0, y_1 \in \mathsf{S}^2$ and find the preimages $f^{-1}(y_0)$ and $f^{-1}(y_1)$. These preimages will consist of a set of closed curves by virtue of f being continuous. Next, it is necessary to choose a direction for the preimages. The direction can be thought of as a parametrisation of a path Γ: $\gamma : I \to \Gamma$, where the direction would be in the direction of increasing $t \in I$, and the path is the preimage. In the case of a disconnected preimage, it is necessary for the direction to be chosen consistently. It can be done in all cases considered in this work, either by choosing points whose preimages are connected, or by following how the preimage changes when the point moves around S^2. In the numerical work, a previously connected preimage can become disconnected during the minimisation process. In these cases the directions of the disconnected components must be consistent with the direction of the connected preimage

just before the disconnection occurs because the deformation is continuous. After all this consideration, the preimages are projected onto a plane; denote this operation by P. The projection must be such that any normal of the plane crosses any connected component of any preimage at most twice. This is easy to do visually, but finding such a plane algorithmically is not trivial. After completing the projection, all the points satisfying the condition $\mathrm{P}\, f^{-1}(y_0) = \mathrm{P}\, f^{-1}(y_1)$ are located and the preimage closer to the plane is marked. The usual convention is to mark it by making a small cut into the projected image so that it looks like it is under the other preimage. Finally, the linking number of the preimages can be defined. It is done with the help of figure 3.1.

Definition 3.19 (Linking number of preimages)**.** Using the method and notation described above, let $y_0 \neq y_1$, the signs of the crossings of preimages $f^{-1}(y_0)$ and $f^{-1}(y_1)$ be defined as in figures 3.1(a) and 3.1(b) and the set of crossings $\mathfrak{C} = \mathrm{P}\, f^{-1}(y_0) \cap \mathrm{P}\, f^{-1}(y_1)$. The *linking number* of the preimages is defined as

$$\widetilde{H}(f) \equiv \tfrac{1}{2} \sum_{i \in \mathfrak{C}} \epsilon(i). \tag{3.17}$$

It is instructive to follow through the procedure described above with an example. Figure 3.1 shows the sequence described above, resulting in linking number of unity.

The linking number of preimages of f equals the value of its Hopf invariant, up to a sign.

Theorem 3.20. *Let $f : \mathsf{S}^3 \to \mathsf{S}^2$. Then, with a suitable choice of direction for the preimages,*

$$\widetilde{H}(f) = H(f) \tag{3.18}$$

Proof. See [40, p. 230]. □

Note that the linking number of preimages is equal to the Hopf invariant for maps defined on $\mathsf{S}^2 \times \mathsf{S}^1$ and T^3 as well [40, p. 230]. Thus the above method can be used to compute the Hopf invariant in these cases as well; as noted in Section 3.5.2, it is no longer invariant unless the real homotopy invariant $t = 0$, but it turns out that it is still conserved under certain

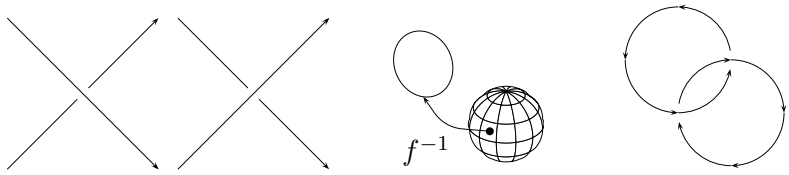

Figure 3.1: Computing the linking number of preimages. Definitions of the signs of the crossings of two distinct preimages are (a) $\epsilon = +1$ and (b) $\epsilon = -1$. Figure (c) represents a point on the target S^2, its preimage on S^3 and the inverse mapping f^{-1} before the projection. In figure (d) the projection of two preimages has been performed, preimages marked according to which one was above before the projection, the directions of the preimages chosen and finally the values of the crossing are marked in to give a system with $H = 1$.

continuous energy minimisation deformations of fields defined on $\mathsf{S}^2 \times \mathsf{S}^1$ [31] and for fields defined on T^3 [34].

A similar construction works for the degree of map $f : X \to Y$ as well. Now the preimages are sets of points instead of loops and there is no notion of crossing. The points must be chosen such that the Jacobian of the map f is non-zero at the preimages. Fortunately, such points occur all over Y. The alternative definition of degree can now be made and shown to equal the previous one.

Theorem 3.21. *Let $f : X \to Y$ be a smooth map, J its Jacobian, $y_0 \in Y$ and $\mathfrak{x}_{y_0} = \{x_0 | f(x_0) = y_0\}$. Let y_0 be such that $J(x) \neq 0 \ \forall x \in \mathfrak{x}_{y_0}$. Then*

$$\deg f = \sum_{\mathfrak{x}_{y_0}} \operatorname{sign} J(x). \tag{3.19}$$

Proof. See [38, p. 57]. □

For field f defined on T^3, a different approach is required. Recall that the invariants t_i count the number of times a preimage travels around the respective S^1 of the T^3. An easy visual method to determine the values t_i is as follows. For each t_i, choose a plane defined by $\hat{e}_i$ and a regular value $p \in \mathsf{S}^2$. Let $\gamma : \mathsf{S}^1 \to \mathsf{T}^3$ again denote the path defined by the preimage

$f^{-1}(p) \in \mathsf{T}^3$. Going around the path, mark all points where γ travels from one side of the plane to the other, numbering them with $j \in \mathbb{Z}$. For each of these points, let $\epsilon(j) = +1$ if γ is directed in the same direction as $\hat{e}_i$ or $\epsilon(j) = -1$ if the directions are opposite. Now, for each i one defines $t_i := \sum_j \epsilon(j)$. In the case where $\gamma(\theta_1) = \gamma(\theta_2) \Leftrightarrow \theta_1 = \theta_2$ (i.e. γ is an injection), it is easy to determine t_i visually: the step of going around γ can now be replaced by finding all points x on the plane, where $f(x) = p$.

During the research at hand, the linking number of preimages has been the predominant method of checking the homotopy of the field. Visually inspecting the preimages is a very fast (at least for low values of H) method and therefore well suited for the task of checking the consistency of the computations. The degree is not quite so fast, but most of the fields in this work will eventually be maps $\mathsf{S}^3 \to \mathsf{S}^2$, so the degree is not that important.

Chapter 4

Models

This chapter introduces the models investigated in this work and applies the results of Chapter 3 to them. It turns out that very few models with topological solitons yield to analytical methods and thus numerical methods are needed. Indeed, this is the case with both models investigated here: the Faddeev-Skyrme model and Ginzburg-Landau model.

4.1 Faddeev-Skyrme model

The Faddeev-Skyrme model was first proposed by L. Faddeev in [12]. It resembles an earlier model, nowadays known as the Skyrme model after T.H.R. Skyrme, which was proposed as a model for baryons in a series of ground-breaking papers [5, 6, 7, 47, 48, 8]. Skyrme developed the model starting from one-dimensional models, eventually formulating a model where the fields form a map $f : \mathbb{R}^4 \to \mathsf{S}^3$. He was then able to show that there is a topological soliton in the system, which he interpreted as a baryon. It has later been shown that the Skyrme model represents the low energy limit of QCD as the number of quark colours increases [49, 50] and it is the topological soliton which is again interpreted as a baryon. These topological solitons are usually called Skyrmions.

The Lagrangian density of Faddeev's model is the same as Skyrme's, but there is one field less than in the Skyrme model, so the fields form a map $f : \mathbb{R}^4 \to \mathsf{S}^2$ instead. This difference may seem small, but the different configuration space makes it possible to consider knotted structures as possible topologically stable static configurations, classified by the Hopf invariant. Indeed, the existence of stable knotted structures was one of Faddeev's key points [12]. There are no knot solitons in the Skyrme

model. Another very interesting result, which shall be presented in more detail shortly, is that the energy of the Faddeev-Skyrme model is bounded from below, the bound is non-zero except for the homotopy class of vacuum solutions and the bound depends on the 3/4 power of the Hopf invariant [51]. Similar bounds can often be constructed for topological solutions, but usually they depend linearly on the respective homotopy invariant. The difference between 3/4 and 1 is important, because linear dependence means that a solution with homotopy invariant $N > 1$, can be decomposed into N infinitely separated solutions with $N = 1$ *without increasing the energy.* In the case of the Faddeev-Skyrme model, this does not occur, due to the sub-linear dependence.

4.1.1 Formulation of the Faddeev-Skyrme model

Let $\Phi \equiv (\phi_1, \phi_2, \phi_3)^T$. Then the Lagrangian density of the Faddeev-Skyrme model can be written as follows.

$$\mathcal{L}_{FS} = c_2 \overbrace{\partial_\mu \Phi^T \partial^\mu \Phi}^{\equiv E_2} + \overbrace{c_4 F_{\mu\nu} F^{\mu\nu}}^{\equiv E_4}, \tag{4.1}$$

$$F_{\mu\nu} \equiv \tfrac{1}{2} \Phi^T \partial_\mu \Phi \times \partial_\nu \Phi \quad \text{or, alternatively} \tag{4.2}$$

$$= \tfrac{1}{2} \epsilon_{abc} \phi^a \partial_\mu \phi^b \partial_\nu \phi^c, \tag{4.3}$$

where c_2 and c_4 are coupling constants. Choosing the usual metric $(+,-,-,-)$ yields the static energy density

$$\mathcal{E}_{FS} \equiv c_2 \|\nabla \Phi\|^2 + c_4 \|F_{jk}\|^2 \tag{4.4}$$

which is perhaps the most important equation of this work. The model evades Derrick's non-existence theorem 2.7 by the virtue of having exactly the correct amount of derivatives in both terms:

$$\left.\frac{\mathrm{d}E_\lambda}{\mathrm{d}\lambda}\right|_{\lambda=1} = -E_2 + E_4 = 0 \qquad \Leftrightarrow \qquad E_2 = E_4 \tag{4.5}$$

$$\left.\frac{\mathrm{d}^2 E_\lambda}{\mathrm{d}\lambda^2}\right|_{\lambda=1} = 2E_2 > 0 \qquad \Leftrightarrow \qquad E_2 > 0. \tag{4.6}$$

Because both E_2 and E_4 are non-negative, the non-existence theorem is circumvented (recall that the theorem assumes $E_j > 0$). The finiteness of energy again ensures the locality of solutions, the topological invariant is

provided by the Hopf invariant (definition 3.12) and (4.5) gives the virial theorem obeyed by any solution of the static field equations. The energy of the Faddeev-Skyrme model is bound from below as follows.

Theorem 4.1 (Vakulenko-Kapitanskii)**.** *Let $\phi : \mathsf{S}^3 \to \mathsf{S}^2$ be a smooth map with Hopf invariant $H(\phi)$ and energy E defined by the Faddeev-Skyrme energy functional. Then $\exists c > 0$ such that*

$$E \geq c\,|H(\phi)|^{3/4}\,. \tag{4.7}$$

Proof. See e.g. [51] or [52]. □

The maximal value of c was not given by Vakulenko and Kapitanskii and it is still unknown, but it was shown by Kundu and Rybakov [53] that $c_{max} > 2^{7/2}3^{3/8}\pi^2\sqrt{c_2c_4} \approx 168.6\sqrt{c_2c_4}$ holds. It has later been suggested by R. S. Ward [52] that $c = 32\pi^2\sqrt{c_2c_4} \approx 315.8\sqrt{c_2c_4}$; the latter has not been rigorously proven (except for the case where the domain is exactly - not just topologically - S^3), but all the numerical work done to date suggests it holds.

The field equations have not been needed until now. They turn out to be analytically intractable, so to prove that there indeed are topologically non-trivial solutions, one must resort to numerical methods. These investigations form the majority of the results presented in this work.

It is not trivial to search for the solutions numerically. Simply supplying the boundary conditions at $r \to \infty$ will (at least typically) yield solutions homotopic to the vacuum, which are uninteresting. Thus, instead of solving the Euler-Lagrange equations by direct integration, a different approach is used. Recall that the Euler-Lagrange equations of the energy density are actually a condition for its extremal; thus any method designed to find the extrema of an integral will be applicable. The methods used in this work are all based on the gradient flow and shall be described in Chapter 5. In order to apply these methods, one needs an initial configuration (or guess) which belongs to the desired (i.e. non-zero) homotopy class. Two such initial configurations are presented in the next section.

It has been noted in Section 2.3.2, that it is not always easy to define a good concept of location for a topological soliton. The Faddeev-Skyrme model is one of the examples, where the energy is not so informative: the solution for $H = 1$ has spherically symmetric energy density, but the fields themselves only have cylindrical symmetry (see [54] for an illustration com-

paring the energy density with the soliton location). Instead, the following definition is used.

Definition 4.2. Let Φ be the field of the Faddeev-Skyrme model and $\Phi(\infty) \equiv \lim_{r\to\infty} \Phi$. The preimage $\Phi^{-1}(-\Phi(\infty))$ is called the *core* of the soliton. This is also identified as the location of the soliton.

Successful numerical attempts to find minimal energy solutions of the Faddeev-Skyrme model had to wait two decades after the model was first proposed; this was most likely due to the system being computationally very difficult, possessing no symmetries that could be used to reduce the dimension below three. The first works regarding the Faddeev-Skyrme model, those of Vakulenko and Kapitanskii [51] and de Vega [55], did not even attempt to find a solution, concentrating on other aspects instead. Enz [56] used a slightly simplified model to obtain straight, infinite vortices and gave qualitative arguments for the existence of closed vortices. Finally, Nicole used a different modified model with $\mathcal{E}_2^{3/2}$ and no $\mathcal{E}_4$ at all in order to construct a scale-invariant theory and found an exact solution [57]. After this, the theory did not receive notable interest before first numerical attempts to find solutions were done. Here follows a short review of these works.

The first ones were by Gladikowski and Hellmund [58], Faddeev and Niemi [59, 60]. The former group used a slightly extended model with extra derivative terms and a potential term, but also reported results when these terms were not present. Their main results were the energy distribution of the $H = 1$ Hopfion, which was unexpectedly found to be concentrated at the origin unlike the core of the Hopfion; they also obtained a $H = 2$ Hopfion and confirmed that such a solution has an energy barrier against decomposition to two $H = 1$ solitons. The main results of the latter group were the (apparently independent) discovery of solitons with $H = 1, 3$. However, the results were qualitatively the same: now, the $H = 1$ energy density was found to be toroidal. The $H = 3$ case had an intriguing knotted shape, but both the toroidal energy density and the knot shape are now believed to be due to an assumption of rotational symmetry or the incorrect handling of boundary conditions, or both. It should be noted that both these groups assumed rotational symmetry in their numerical work.

The first fully three dimensional numerical analyses were those of Battye and Sutcliffe [54, 61], and Hietarinta and Salo [62, 63]. The former group confirmed the earlier $H = 1, 2$ results, but found a disagreement

with the $H = 3$ Hopfion: their $H = 3$ Hopfion is not rotationally symmetric, but instead a twisted torus. They also found Hopfions of H up to 8 and discussed the possible mechanisms behind the rich variety of solitons in the model. The latter group also found Hopfions up to $H = 7$, but this time using quite different initial configurations than the others. The results were found to agree with those of Battye and Sutcliffe, therefore providing a strong independent confirmation of the earlier results. The latter group used a very versatile method of creating linked configurations and also developed a very powerful and informative method of visualising Hopfions. Both groups discovered that the $H = 7$ Hopfion has a knotted core, finally realising the the original idea of Faddeev [12].

To summarise these works, it was found that the solution of Hopf invariants one and two have a toroidal soliton core, while higher values provide increasingly complex core shapes, ultimately yielding the first real knot soliton at $H = 7$. Numerical work in this direction has since expanded considerably, not only by the results presented in this work, but also by that of Sutcliffe, who has found Hopfions up to $H = 16$ [64].

Although there have been many numerical results, a definite, rigorous proof of the existence of Hopfions was not available until Lin and Yang managed to prove the following [65].

Theorem 4.3. *Let Ω be a bounded, smooth domain in $\mathbb{R}^3$, $E(\cdot)$ the energy,*

$$X_\Omega = \{\Phi : \mathbb{R}^3 \to \mathsf{S}^2 | E(\Phi) < \infty \text{ and } \Phi((\operatorname{int}\Omega)^c) = \text{ constant}\}, \tag{4.8}$$

and $q \in \mathbb{Z}$. Then there exists a field Φ_q for which $H(\Phi_q) = q$ and

$$E(\Phi_q) = \min\{E(\Phi) | \Phi \in X_\Omega \text{ and } H(\Phi) = q\}. \tag{4.9}$$

Proof. See [65]. □

They also provided a slightly weaker statement for unbounded domains. In that case the values of d are restricted to an (unknown) infinite subset of $\mathbb{Z}$. As a byproduct, Lin and Yang were also able to show that the energy of the minimal energy configuration is bound not only from below (theorem 4.1) but also from above.

Theorem 4.4. *Using the notation of theorem 4.3, there exists $0 < C \in \mathbb{R}$*

such that

$$E(\Phi_q) \leq C\,|q|^{3/4}\,. \tag{4.10}$$

Proof. See [65]. □

No value of C was given by Lin and Yang, but an upper limit for it was later found [66] and [67]. By using numerical integration at certain stages of the derivation, Hirayama et al. provided the lower estimate, $C = 6233\sqrt{c_2 c_4}$.

4.1.2 Initial configurations

Naturally, all the works mentioned above have their methods of generating initial configurations of the desired Hopf invariant. The method described and used by Sutcliffe [64] is perhaps the most flexible one, but the method used in this work is due to [58, 68]. It is worth mentioning that [68] considered an altered model without $\mathcal{E}_2$ and $\mathcal{E}_4^{3/4}$ to provide scale invariance. They were able to give an exact solution of Hopf invariant one and construct a completely integrable model admitting Hopfions. The initial configuration of [58, 68] can be written as follows.

Theorem 4.5. *Let η, ξ, φ be the toroidal coordinates of one-point compactified $\mathbb{R}^3$, related to the cartesian ones by*

$$\begin{aligned} x_1 &= \frac{\sinh(\eta)\cos(\varphi)}{\Delta}, \qquad & x_2 &= \frac{\sinh(\eta)\sin(\varphi)}{\Delta}, \\ x_3 &= \frac{\sin(\xi)}{\Delta}, & \Delta &= \cosh(\eta) - \cos(\xi), \end{aligned} \tag{4.11}$$

$p, q \in \mathbb{Z}$, and $g\colon [0,\infty) \to [0,1]$ monotonic. Define the map $\chi : \mathsf{S}^3 \to \mathsf{S}^2$ by

$$\begin{aligned} \chi = \big(&g(\eta)\cos(p\xi), g(\eta)\sin(p\xi), \\ &\sqrt{1-g\big(\eta\big)^2}\cos(q\varphi), \sqrt{1-g\big(\eta\big)^2}\sin(-q\varphi)\big). \end{aligned} \tag{4.12}$$

Now $\deg \chi = pq$.

Proof. See [68]. □

Corollary 4.6. *Using the notation of theorem 4.5, define*

$$\Phi = \begin{pmatrix} 2g(\eta)\sqrt{1-g(\eta)^2}\cos(p\xi+q\varphi) \\ 2g(\eta)\sqrt{1-g(\eta)^2}\sin(p\xi-q\varphi) \\ 2g^2(\eta)-1 \end{pmatrix}. \tag{4.13}$$

Now the Hopf invariant of Φ *is*

$$H(\Phi) = pq. \tag{4.14}$$

Proof. The result follows from theorem 3.17. □

There are many simplifications and choices to be made in (4.12). One possibility is to take $p = q = 1$, which gives the original map used by Hopf [69] to prove that there is a map $\mathsf{S}^3 \to \mathsf{S}^2$ which is not homotopic to the constant map. One can also denote $r = \|x\|$, choose

$$g(\eta) = g(x,y,z) = \frac{\sqrt{(r^2+1)^2 - 4(x_1^2+x_2^2)}}{r^2+1}, \tag{4.15}$$

and identify $n_1 = \phi_2$, $n_2 = \phi_1$, and $n_3 = \phi_3$ to obtain the field $\vec{n}$ used in [62, 63].

The initial configuration used in our vortex investigation is slightly different due to the altered topology of the system. The configuration can be thought of as the same as in theorem 4.5, but that the toroidal core has been cut and the torus straightened into a cylinder. Using cartesian coordinates and two integers m, n, the form of the field ϕ is

$$\Phi = \begin{pmatrix} \sqrt{1-f(\rho)^2}\,\cos(m\theta + 2\pi nz/L) \\ \sqrt{1-f(\rho)^2}\,\sin(m\theta + 2\pi nz/L) \\ f(\rho) \end{pmatrix}, \tag{4.16}$$

where L is the box length in the z-direction and f is just some profile function with $f(0) = -1$, $f(\infty) = +1$. Sometimes the initial configuration was also slightly bent in order to reduce the computation time required for energy minimisation. More details and motivation are discussed in [31]. Since the domain is no longer S^3, but $\mathsf{S}^2 \times \mathsf{S}^1$ instead, the topological invariants are s_1 and s_2 as given by theorem 3.18. Using the integral formula for the

degree (3.6) or inspecting the configuration visually using the method of theorem 3.21, one obtains $s_2 = m$. As was seen in 3.5.2, the linking number of preimages remains well defined and is equal to the Hopf invariant, although its value is no longer homotopy invariant. Simple computation of the linking number of these initial configurations gives $H = mn$.

For the systems investigated in [34] the domain of the fields is T^3 and the topological classification is that of theorem 3.18. The initial configurations, are constructed using (4.16) with $m = 1$ and $n = 6$. In two of the computations of [34], several identical vortices were packed in a tight formation into the computational lattice. Using the method described in section 3.5.3, it is straightforward to check that for (4.16) $t_1 = t_2 = 0$ and $t_3 = 1$. For the packed formations of vortices these are simply multiplied by the number of vortices. The Hopf invariant can also be calculated for these configurations, but as was seen in [34], it is conserved only in special cases.

4.2 The Ginzburg-Landau model

This section introduces the Ginzburg-Landau model. It is usually used to describe (planar) superconductors near the critical temperature, but it is also the static limit of the Abelian Higgs model with two complex Higgs scalars. The model is widely known for its topological solitons in two dimensions, called Abrikosov vortices according to the work by Abrikosov [4]; indeed, the 2003 Nobel prize in physics was awarded to Abrikosov, Ginzburg and Leggett for work related to the Ginzburg-Landau theory and its vortices.

It is possible to derive the Faddeev-Skyrme model from Ginzburg-Landau model using a derivative expansion [27], but this method does not allow for investigation of solitons in the Ginzburg-Landau model since it does not correspond to any parameter limit. Instead, the Faddeev-Skyrme model can be embedded in the Ginzburg-Landau model by a change of variables, as shown by Babaev et al. [29]. This embedding makes an intriguing connection between the Faddeev-Skyrme and Ginzburg-Landau models. However, the topological features of the Faddeev-Skyrme model cannot be directly applied without further considerations as shall be demonstrated in Sections 4.2.2 and 4.2.3.

The next few results relate to the Ginzburg-Landau model in general.

After those, the special cases of Abrikosov vortices and the embedding of the Faddeev-Skyrme model are considered. In what follows, only the energy density will be defined and the Lagrangian density will be left undetermined. There is a reason for this. The Ginzburg-Landau energy density is not unique to the Ginzburg-Landau model: the same energy density occurs as the static energy density of the Abelian Higgs model as well. Since this work does not deal with the dynamical model, but only the static one, deciding which time-dependent part to use is not necessary.

The usual version of Ginzburg-Landau model has one complex field, but it can be extended to any number of fields; in this work, the version with two fields has been used, with a few comparisons with the usual model of one field. In the following paragraphs and sections, therefore, the notation of Ψ always refers to the two-component model, ψ_α to one of these components and ψ to the one component model.

Definition 4.7 (Ginzburg-Landau energy)**.** Let $\psi_\alpha : \mathbb{R}^D \to \mathbb{C}$ and $\vec{A} : \mathbb{R}^D \to \mathbb{R}^3$ be the fields, $\vec{D}_\alpha \equiv \nabla - ig_\alpha \vec{A}$ the covariant derivative and $g_\alpha \in \mathbb{R}$ coupling constants. The Ginzburg-Landau energy density is

$$\mathcal{E}_2 \equiv \tfrac{1}{2}\|\vec{D}_1\psi_1\|^2 + \tfrac{1}{2}\|\vec{D}_2\psi_2\|^2 \tag{4.17}$$

$$\mathcal{E}_4 \equiv \tfrac{1}{2}\|\nabla\times\vec{A}\|^2 \tag{4.18}$$

$$\mathcal{E}_0 \equiv \tfrac{1}{2}V\big(\psi_1,\psi_2\big) \tag{4.19}$$

$$\mathcal{E}_{GL} \equiv \mathcal{E}_2 + \mathcal{E}_4 + \mathcal{E}_0 \tag{4.20}$$

with some potential V. Usually, and always in this work, the potential has the form

$$\begin{aligned} V(\psi_1,\psi_2) = {} & c_1|\psi_1|^4 + c_2|\psi_2|^4 + c_3|\psi_1|^2|\psi_2|^2 \\ & + b_1|\psi_1|^2 + b_2|\psi_2|^2 + a_0. \end{aligned} \tag{4.21}$$

It should be noted, that various different notations have been used for the Ginzburg-Landau model. For example, in condensed matter physics, it is usual to write

$$\mathcal{E} = \tfrac{\hbar^2}{2m}\Big\|\big(\nabla - \frac{2e}{c\hbar}\vec{A}\big)\psi\Big\|^2 + \tfrac{1}{2\mu_0}\|\nabla\times\vec{A}\|^2 + \tfrac{1}{2}b\,|\psi|^4 - a\,|\psi|^2\,,$$

or a variation thereof. There are physical reasons for this kind of formula-

tion; most notably the two experimentally important values

$$\lambda \equiv \frac{c}{e}\sqrt{\frac{mb}{2\mu_0 a}} \quad \text{and} \quad \xi \equiv \hbar/\sqrt{2ma},$$

called the penetration depth and coherence length. However, for mathematical treatment, the form in (4.17) is more appropriate. For a single field, it can be further simplified as shall be seen in Section 4.2.1.

As usual, the first step in determining the possibility of topological solitons in a model is to apply Derrick's theorem. However, the situation is no longer the simple one with just scalar fields: the introduction of the gauge field $\vec{A}$ makes things significantly more complex. The exact details of how the situation changes will not be covered here, but, as shall be seen in Section 4.2.1, the gauge field makes it possible to have a finite energy even for the gradient term: it is possible that $\vec{D}\psi = 0$ even if $\nabla\psi \neq 0$. The Abrikosov vortex discussed below is one such situation. For the application of Derrick's theorem, however, one needs to know the scaling behaviour of the gauge field. It is necessary for the gauge field to behave like a derivative which can most easily be understood from the differential geometric formulation, where the gauge field becomes a 1-form. From Derrick's theorem one obtains the following necessary condition for the existence of topological solitons in Ginzburg-Landau model

$$\begin{cases} E_4 & = E_0 \\ E_4 + 3E_0 & > 0, \end{cases} \qquad \text{when } D = 2, \text{ and} \tag{4.22}$$

$$\begin{cases} E_4 & = E_2 + 3E_0 \\ E_2 + 6E_0 & > 0, \end{cases} \qquad \text{when } D = 3. \tag{4.23}$$

The locality condition of definition 2.5 must be checked separately for all prospective topological solitons, but for any finite energy configuration it will necessarily be satisfied. The last requirement of the existence of a topological invariant is dependent on the value of D and therefore will only be discussed after D is fixed.

It should be emphasised, that the fields of the Ginzburg-Landau model are maps to $\mathbb{R}^2 = \mathbb{C}$ and therefore it is perfectly possible that $\Psi = 0$ at one or even all points of the domain. This implies that it is possible to violate the assumptions of Derrick's theorem and have any or all of $E_j = 0$. The

implications of this shall be evident in Section 4.2.2.

4.2.1 Abrikosov vortex

In this section, the Ginzburg-Landau model with one complex field only is considered. The target space $\mathbb{C}$ implies that the relevant homotopy group is $\pi_D(\mathcal{V})$, where $\mathcal{V}$ is defined by the potential V. If the $\mathcal{V}$ is too large (like the whole $\mathbb{C}$) or too small (like just one point), the homotopy group will be trivial. There is a very important case, where

$$D = 2, \quad g_1 = 1 \quad \text{and} \quad V(\psi) = \frac{\eta}{8}\big(|\psi| - 1\big)^2.$$

The vacuum is now $\mathcal{V} = \mathsf{S}^1$ and hence the relevant homotopy group $\pi_1(\mathsf{S}^1)$; a member of $\pi_1(\mathsf{S}^1)$ is often called a *winding number*. Note that there is just one parameter in the model: η. This is the only free parameter of the one-component model, all the others can be scaled away. Of course, there are different ways to scale away the dependent parameters and any parameter can be chosen as the independent one. The form presented here is perhaps the most common.

The vortex configurations of winding number unity have rotational symmetry [58, 59], so it is easiest to describe the fields in polar coordinates, when they become functions of only the radial coordinate, r. The fields have the following properties: $\psi(0) = \vec{A}(0) = 0$, $|\psi(\infty)| = 1$ and $\vec{A}(\infty) = 0$. Due to the rotational symmetry of the system, it is natural to call the origin the location of the vortex, but for larger winding numbers, origin is not always a special point, so another definition is needed. The natural choice is the property of the scalar field at the origin: the Abrikosov vortex location is defined by the preimage $\psi^{-1}(0)$. This coincides with origin for the unit winding vortex, but it works also for other vortices.

The value of $\eta = 1$ splits the parameter space in three: the fields where $\eta < 1$ are called type-I, fields where $\eta > 1$ are called type-II and the case $\eta = 1$ is a special one; it is often called the critical coupling. For the superconductor interpretation of the theory, the properties of type-I and type-II fields are significantly different. The phase diagram of type-I superconductors have a single critical temperature above which the superconductivity is lost while type-II superconductors have two critical magnetic fields B_{c_1} and B_{c_2} with $B_{c_1} < B_{c_2}$. Below B_{c_1}, just the superconducting phase is present, but for field strengths between B_{c_1} and B_{c_2}, a mixture of normal

and superconducting phases appears. This is called a mixed state. The regions of the normal phase are the cores of the Abrikosov vortices and if allowed to relax, they form the famous Abrikosov lattice [4]. The properties of the vortices are also different, but the details depend on the selected time-dependence.

Without the time dependence specified, it can only be determined that vortices with positive (negative) winding attract if $\eta < 1$ and repel if $\eta > 1$ – obviously at $\eta = 1$ they do neither, but are in an equilibrium and the vortices can exist anywhere on the plane. Vortices with opposite winding always attract and annihilate. Therefore, if the total winding number is zero, the configuration is homotopic to the vacuum.

There is a second important difference between the critical and non-critical vortices. For a number of field theories, there is a lower bound for the energy, which relates the energy and homotopy class of the field at the boundary. These bounds are called Bogomolny bounds due to the observations in [37]. For critical vortices in the present model, the bound becomes $E \geq N\pi$, where $N \in \pi_1(\mathsf{S}^1)$ is the homotopy class of ψ and E the total energy.

4.2.2 Ginzburg-Landau model in three dimensions

The two dimensional Abrikosov vortices can trivially be extended into three dimensions, if the system is made translation invariant in the new dimension. This extension, does not change the topological character of the model. For examples of more complicated ways of embedding the two dimensional vortices in three dimensions, see [70].

Things change, however, if the third dimension is added without any symmetry requirements. The topological features of the system must then again be determined by the boundary values and the vacuum manifold. The vacuum manifolds used in this work are $\mathcal{V} = \mathrm{SU}(2)$ and $\mathcal{V} = \mathrm{U}(1) \times \mathrm{U}(1)$. Topologically $\mathrm{SU}(2) = \mathsf{S}^3$ and $\mathrm{U}(1) \times \mathrm{U}(1) = \mathsf{T}^2$, so the relevant homotopy groups become $\pi_2(\mathsf{S}^3) = 0$ and $\pi_2(\mathrm{T}^2) = 0$. Thus the search ends: there is no non-trivial topology. However, this is changed when the theory is considered as a constrained one, and the vacuum manifold is no longer the sole player in the topology of the system.

One way to proceed is to require that $\|\Psi\| = 1$ everywhere, making the fields maps $\mathbb{R}^3 \to \mathsf{S}^3$. Now, by the arguments of Section 3.3, the relevant homotopy group becomes $\pi_3(\mathsf{S}^3) = \mathbb{Z}$ and there is a possibility of topological

solitons.

There exists an interesting change of variables for the constrained version due to Babaev et al. [29]. Recall the definition 3.15 of the Hopf map, denote it again with h and let $g_1 = g_2 = g$. It should be noted that the original work in [29] and that presented in [32] used $g_1 = -g_2 = g$, but this is equivalent to global gauge rotation $\psi_2 \to \overline{\psi_2}$, which can be done without changing anything else. The requirement $\|\Psi\| = 1$ is also relaxed so that the only constraint on Ψ is $\|\Psi(x)\| > 0$ everywhere. It is now convenient to define $\chi : \mathsf{S}^3 \to \mathsf{S}^2$ by $\chi \equiv \Psi/\|\Psi\|$ and define the new fields $\Phi, \rho, \vec{C}$ as follows.

$$\begin{cases} \rho & \equiv \sqrt{\frac{1}{2}\big(|\psi_1|^2 + |\psi_1|^2\big)}, \\ \vec{C} & \equiv 2\Big(i\big(\overline{\chi}^T \nabla \chi - \chi^T \nabla \overline{\chi}\big) - 2g\vec{A}\Big), \\ \Phi & \equiv h(\chi). \end{cases} \tag{4.24}$$

Using these new variables, the energy density becomes

$$\begin{aligned} \mathcal{E} = {} & \tfrac{\rho^2}{4}\|\nabla \Phi\|^2 + \|\nabla \rho\|^2 + \tfrac{\rho^2}{16}\|\vec{C}\|^2 + V\big(\rho, \Phi\big) \\ & + \tfrac{1}{32g^2}\|\Phi^T \partial_k \Phi \times \partial_l \Phi + \partial_k C_l\|^2. \end{aligned} \tag{4.25}$$

This is the form derived by Babaev et al. [29] and the embedding of Faddeev-Skyrme model into the two-component Ginzburg-Landau model is quite explicit: when $\vec{C} = 0$, it becomes the Faddeev-Skyrme model, except that there is a potential V; the presence of a potential does not alter the topology of the system and if also $V = 0$ it becomes exactly the Faddeev-Skyrme model.

The next topic to explore is again Derrick's theorem. Recalling (4.23), one is tempted to conclude that this model does indeed support topological solitons. This is, however, not the case. Until now, just the topology of the field Φ has been considered, but a glance at (4.17) reveals that the balancing term in (4.23), $\mathcal{E}_4$, does not depend on Φ (or Ψ) at all! It is solely a function of the gauge field $\vec{A}$. Therefore, nothing ensures that $\mathcal{E}_4 > 0$, as assumed by Derrick's theorem. Indeed, it has been be rigorously proven [71] that for the energy density (4.25) there are no stable solutions which are global minima of the Ginzburg-Landau energy within their respective homotopy classes; i.e. for a given homotopy class, the global minimum of energy is always zero. This is ultimately due to the term $\mathcal{E}_4$ having no compelling

reason to be non-zero. This is rather unfortunate, but the possibility of local minima remains. While these would not normally be considered topological solitons, in the classical theory they are stable against small perturbations. Therefore they are interesting objects as well, if they exist. Their possible existence has been investigated in [32].

There are several ways to possibly escape this conundrum. One way is to enforce a non-zero (possibly external) magnetic field into the system, or to introduce a phase winding for Ψ at $r \to \infty$, which will force $\vec{A}$ to compensate lest the covariant derivative term yields an infinite energy. These two methods do not seem to have been investigated. A third method is to modify the energy density so that it is energetically unfavourable for $\mathcal{E}_4$ to be zero. There are various ways of achieving this. Most notable of these are the introduction of an Andreev-Bashkin type term [72] and an approach based on modifying the metric of the configuration space [73]. The last of these methods will be discussed next.

4.2.3 Ward's modification

The idea behind the Ward's modification [73] is simple. The symmetry of Φ consists of a local U(1) gauge symmetry and a global SU(2). By altering the metric of the SU(2) part, the energy density gains an additional term

$$\mathcal{E}_W = \tfrac{1}{2}\kappa^2 \|\Phi^\dagger \vec{D}\Phi\|^2, \tag{4.26}$$

where $\kappa > 0$ is a new parameter in the system. The potential must now be SU(2) symmetric

$$V = \tfrac{1}{2}\eta(\|\Phi\|^2 - 1)^2. \tag{4.27}$$

The limit $\kappa, \eta \to \infty$ recovers exactly the Faddeev-Skyrme model, because at this limit, $\|\Phi\| \to 1$ and $\vec{C} \to 0$ everywhere. Therefore, it is reasonable to ask, if the Hopfions of Faddeev-Skyrme model survive when κ, η are finite. It turns out, they do [73]. The proof of [71] holds even with the additional term, and, therefore, any Hopfions are necessarily only local minima of their respective homotopy classes. This modified model has been further investigated in [33].

4.2.4 Initial configuration

Recall that the eventually interesting object will be the Hopfion, the configuration of Φ, not Ψ. Therefore, all the initial configurations used in studying the three dimensional Ginzburg-Landau model have been constructed using the theorem 3.17: any map χ for which $\deg \chi = n \in \mathbb{Z}$, the Hopf map h and field configuration $\Phi \equiv h \circ \chi$, it will follow that $H(\Phi) = n$ as well. There are numerous ways of constructing maps of desired degree. The one used here is the χ given in theorem. 4.5; the value of ρ has been fixed to a constant (usually $\rho = 1$) for all initial configurations. It should be noted that even though the initial configuration is here presented in terms of variables used by Babaev et al. [29], all the computations have been done in Ψ, $\vec{A}$ only.

The initial configuration for $\vec{A}$ needs to be determined as well. For pure Ginzburg-Landau computations, the initial configuration was simply $\vec{A} = 0$, but for the modified model, $\vec{A}$ was initialised according to the condition $\Phi^\dagger \vec{D} \Phi = 0$. Where the solution is not real, only the real part is used.

Chapter 5

Numerical methods

It was noted in the beginning of Chapter 4 that numerical methods are often needed to study topological solitons. The Euler-Lagrange equations are not integrable analytically, so numerical integration is required. Regardless of the numerical method, some kind of discretisation is necessary.

In principle, one can try to integrate the Euler-Lagrange equations directly, given some boundary conditions. However, as was noted in Section 4.1, this tends to lead to solutions homotopic to the vacuum, which are not interesting. This is especially true for constrained fields, which have no enforcing topology at the boundary; for unconstrained fields and topologically constrained boundary conditions, the result of a direct integration should, in principle, provide a configuration of the respective homotopy class. There is a caveat: the equations of motion are often very non-linear and stiff, and direct integration may, therefore, be extremely sensitive to the initial (boundary or otherwise) values.

In this chapter, the following notations are used. For a variable $x \in \mathbb{R}^D$, the symbol $\hat{x}$ is a point on the corresponding lattice, h is the distance between two lattice points (the same in all directions and all over the lattice), M is the number of fields, counting both scalar and gauge and N is the number of lattice points. In a typical computation in this work, $\mathsf{N} \in [120^3, 720^3]$. If Φ denotes the fields, the gradient of a discrete functional with respect to each field at each lattice point will be denoted by ∇_Φ. Thus ∇_Φ gives a vector of MN components.

5.1 Discretisation

The discretisation scheme chosen in this work is the finite difference method. It is built on the definition of derivative: in its simplest form, the finite difference method simply makes a substitution for all derivatives $\partial_j f(x) \to (f(\hat{x} + h\hat{j}) - f(\hat{x}))/h$ and changes the integrals $\int \mathrm{d}x \to \sum h$ in the energy functional (and similarly for higher derivatives if there are any) - in practise, more sophisticated methods are often used.

The discretisation used in [30, 31, 34] is fully described in [62, 63]. In short, the second order term was discretised on links by simple forward differences and the fourth order term was discretised on plaquettes (again by forward differences); for example $F_{jk}(x)$ is discretised on the $\hat{j}\hat{k}$-plaquette as follows

$$\phi_a(x) \to \tfrac{1}{4} \sum_{l,m=0}^{1} \phi_a(\hat{x} + hl\hat{j} + hm\hat{k}) \tag{5.1}$$

$$\partial_j \phi_a(x) \to \tfrac{1}{2h} \sum_{l=0}^{1} \big(\phi_a(\hat{x} + h\hat{j} + hl\hat{k}) - \phi_a(\hat{x} + hl\hat{k})\big). \tag{5.2}$$

During the minimisation process, the algorithms presented later in this chapter do not guarantee that the norm of the unit-vector field Φ is preserved. Indeed, it was observed that it never is. Therefore, some method of keeping the norm fixed was necessary. The solution chosen in [62] was to renormalise the field after each iteration and this method was used also in the work presented here.

This discretisation works quite well for scalar fields and problems like the question of the existence of topological solitons, where it is not necessary to find the most accurate solution possible. For gauge fields, the situation is different. Using the same discretisation for gauge fields will destroy the gauge invariance of the model. Fortunately, Wilson has devised a way of discretising gauge fields gauge invariantly [74]. The method is fully described in [32], but the crucial point is the use of exponentials as follows. If one denotes a lattice point by $\hat{x}$, the covariant derivative term becomes

$$\begin{aligned}\|(\nabla - ig\vec{A})\psi_k(x)\|^2 \;\to \sum_{j=1}^{3} \big(&\overline{\psi_k}(\hat{x}+h\hat{j})\psi_k(\hat{x})e^{ihgA_j(\hat{x})} \\ &+ \psi_k(\hat{x}+h\hat{j})\overline{\psi_k}(\hat{x})e^{-ihgA_j(\hat{x})} \\ &- \overline{\psi_k}(\hat{x}+h\hat{j})\psi_k(\hat{x}+h\hat{j}) - \overline{\psi_k}(\hat{x})\psi_k(\hat{x})\big), \quad (5.3)\end{aligned}$$

and the magnetic field energy

$$\|\nabla \times \vec{A}(x)\|^2 \;\to -6 + \sum_{j,k=1}^{3} e^{iF_{jk}(\hat{x})}, \quad (5.4)$$

where

$$F_{jk}(\hat{x}) = A_j(\hat{x}+h\hat{k}) - A_j(\hat{x}) - A_k(\hat{x}+h\hat{j}) + A_k(\hat{x}). \quad (5.5)$$

It is easy to see that (5.3) and (5.4) indeed are exactly gauge invariant under the discretised gauge transformation

$$A_j(\hat{x}) \to A_j(\hat{x}) + (\theta(\hat{x}+h\hat{j}) - \theta(\hat{x}))/h \quad (5.6)$$

$$\psi_k \to \psi_k \mathrm{e}^{ig\theta(\hat{x})}. \quad (5.7)$$

The additional term introduced in Section 4.2.3 is discretised similarly, for details, see [33]. The accuracy of the energy thus achieved on the continuum limit is $\mathcal{O}(h)$, which is quite sufficient for a study of existence.

It is also perhaps worth noting that after discretisation the fields are independent unknowns in each lattice point, thus an energy density with M independent fields and a lattice of N points yields a discretised energy which is a function of MN variables. The discretised energy functional is a function of the discretised fields Ψ, $\vec{A}$ at each lattice point, so the Euler-Lagrange equations reduce to the gradient of the energy density (taken with respect to the fields at each lattice point).

For dynamical systems, the same method can be used for time derivatives as well, as is done in lattice QCD, but the usual way of discretisation is to do the above for spatial derivatives, then find the Euler-Lagrange equations for the space-discretised Lagrangian and finally discretise the time evolution separately.

5.2 Algorithms

One possible – and the one used here – approach to investigating the existence and properties of topological solitons is to treat the energy functional as an optimisation problem. It is well known that if the minimum of the energy functional is found, it will necessarily be a solution of the full dynamical model as well, so the approach is valid. For a Lorentz invariant theory, this soliton can then be set in motion by a Lorentz transformation.

In the numerical search of a minimiser of the objective function E, no single algorithm is always the best by all criteria. The accuracies of the gradient based algorithms are generally equally good if the convergence criterion is chosen suitably, but the speed of convergence of an algorithm depends on both the initial guess and the objective function, with no reliable way of telling which algorithm will converge fastest. Sometimes it is possible to give an upper limit for the number of iterations needed to reach a solution, like for quadratic functions and some conjugate gradient methods [75, p. 64]. Even that is not a reliable way of comparing the algorithms because this is a limit, not always the actual number used. Also, in the present work, the problem is not quadratic. It is usually not even possible to know how long a single iteration will take. Consider an algorithm using a line search (defined in Section 5.2.1). The number of line searches needed per iteration is not known *a priori* and can change from iteration to iteration, so it is not possible to estimate the total time spent doing the line searches. Thus, the only way of choosing one algorithm over others is to see how they perform with the specific task at hand.

There are also constraints on the selection of the algorithm: their memory requirements are different, so if the optimisation problem is very large, the memory requirements may prevent the use of some of the algorithms.

All the algorithms used in this work use a gradient based minimisation algorithm. There are algorithms that work without gradients, but they are generally much slower and therefore gradient based algorithms are preferable whenever the gradient information exists (or can reliably be estimated). The drawback is that gradient based algorithms will find a minimum, possibly local, and cannot proceed further. For global minimisation, something else is needed. One very popular example of a non-gradient algorithm suitable for global minimisation is provided in Section 5.2.5.

If the initial guess is not a solution already, all these algorithms will find a minimum. If the initial guess is a solution, these algorithms do

nothing regardless of the nature of the stationary point. There is usually no fear of this happening for two reasons. Numerical inaccuracies will most likely be such that the gradient is not exactly zero even for a solution and the algorithms proceed down from the maximum or saddle point. It is also usually trivial to change the initial guess slightly to provide a similar nudge. Of course, such accidentally found solution might prove very valuable if, for example, its functional form is known.

The various algorithms all need a condition when to stop the algorithm. A proper discussion of this is easier after the algorithms have been introduced and some numerical considerations discussed. Therefore, the discussion of convergence conditions of the algorithms will be delayed to Section 5.3.3.

5.2.1 Line search

The algorithms presented in the following sections rely heavily on the concept of *line search*. This means that, given the objective function E, some starting point x and direction d, one is to find the value τ for which $E(x+\tau d)$ obtains its minimum value. The exact details of how this is accomplished are largely irrelevant. Apart from possible numerical inaccuracies and rounding errors (which are not due to the method), the only practical difference between line search algorithms is their speed. There is no single best algorithm, but some of the often used ones are Fletcher's method [75] and ordinary bisection method. In principle, any one-dimensional minimisation algorithm could be used.

5.2.2 Steepest descents

The method of steepest descents is also known as gradient flow. It is based on the fact that the objective function $E(\Phi)$ decreases in the direction $-\nabla_\Phi E(\Phi)$. In its simplest form, the objective is reached by taking small steps until the minimum is found. Let $E(\Phi)$ be the objective function (in this work it will always be the energy, hence the symbol E), λ_k the step sizes and Φ_0 the initial guess. Note that Φ_k is the total set of variables E depends on; it is not the kth component of Φ (which is denoted by ϕ_k).

1: $k \leftarrow 0$
2: **while** not converged **do**
3: determine λ_k in some manner

4: $\Phi_{k+1} \leftarrow \Phi_k - \lambda_k \nabla_{\Phi_k} E(\Phi_k)$
5: $k \leftarrow k + 1$
6: **end while**

The determination of λ_k in step 3 can be done in different ways. The simplest option is to use a sufficiently small constant value. A more sophisticated method uses a line search to find the optimal value of λ for each step; however, unlike for the conjugate gradient and Newton methods, for steepest descents line searches are not required. The version used in [32, 33] uses a compromise between the two. The line search eventually boils down to taking many steps with different values of λ, which can be time consuming, depending on how many steps are needed to converge the line searches. The compromise used here starts with some value for λ. At each iteration, the old value of λ is first tried and if that results in a decreased objective function value, λ is updated to twice its old value and that will be used for the next iteration. If the first try results in an increased objective function value, λ is decreased to $\lambda \rightarrow 0.55\lambda$ and a new attempt is made; this is repeated until the step results in a lower objective function value. The resulting λ is then used for the next iteration.

5.2.3 Conjugate gradient algorithms

While the gradient method is mathematically well understood, simple to implement in a computer, easy to understand and guaranteed to find the minimum, it is also sometimes very inefficient. To compensate for this disadvantage, a set of algorithms called the conjugate gradient algorithms have been developed. Like the gradient method, they also start the optimisation process in the gradient direction, but also remember something about all the previous directions the algorithm has used, and utilise this information when taking the next steps. The various conjugate gradient algorithms differ only in the way the previous gradients are used. The perhaps most commonly used ones are due to Fletcher and Reeves [76] and Polak and Ribière [77], but others exist as well.

For a quadratic problem and exact line searches, it can be shown that the Fletcher-Reeves algorithm converges in a number of steps equal to or less than the number of variables [75]. This is not true for a simple gradient algorithm. This is a strong motivation for using these algorithms for quadratic problems, but it turns out they are often quite effective for other problems as well.

The conjugate gradient method can be written as an algorithm as follows, using the notation of Section 5.2.2. In the algorithm the vector d_k is called the search direction.

1: $k \leftarrow 0$
2: $\beta_{-1} \leftarrow 0$
3: $d_{-1} \leftarrow 0$
4: **while** not converged **do**
5: $\quad d_k \leftarrow -\nabla_{\Phi_k} E(\Phi_k) + \beta_{k-1} d_{k-1}$
6: $\quad$ perform line search to find λ_k which minimises $E(\Phi_k + d_k \lambda_k)$
7: $\quad \Phi_{k+1} \leftarrow \Phi_k + \lambda_k d_k$
8: $\quad$ update β_k according to the chosen scheme
9: $\quad k \leftarrow k + 1$
10: **end while**

The Fletcher-Reeves scheme for updating β_k is

$$\beta_k = \frac{\|\nabla_{\Phi_k} E(\Phi_{k+1})\|}{\|\nabla_{\Phi_k} E(\Phi_k)\|} \tag{5.8}$$

and the Polak-Ribière scheme is

$$\beta_k = \frac{(\nabla_{\Phi_k} E(\Phi_{k+1}) - \nabla_{\Phi_k} E(\Phi_k))^T \nabla_{\Phi_k} E(\Phi_{k+1})}{\|\nabla_{\Phi_k} E(\Phi_k)\|}. \tag{5.9}$$

In practise, if the objective function is not quadratic, the algorithm may run out of conjugate directions; it may also become exceedingly slow if it wanders to a region where the convergence is far from quadratic. For these reasons, the algorithm is usually modified so that for every $k \equiv 0 \pmod{n}$, the search direction is reset to $d_k = -\nabla_{\Phi_k} E(\Phi_k)$. Usually n is taken to be the number of unknowns in the system, but a smaller value is also sometimes used. In [32, 33], restarts were performed whenever the algorithm failed to take a step despite the gradient being non-zero. Due to the implementation of the algorithm, this can happen either due to numerical inaccuracies or if the function is very far from quadratic in the search direction. In practise, this happens a few times per each minimisation process and also whenever computing had to be halted. At this point, only the fields Φ and $\vec{A}$ were saved to disc so the conjugate information was lost. The search direction would have been reset when $k = n$, but that many iterations were never

necessary. The two of the three versions of conjugate gradient algorithms used in this work are derived from the GNU Scientific Library, version 1.9 [78]. In [62, 63, 34] the line search was replaced by heuristic or constant values for λ_k, and restarts were performed only when the computing was halted. Nevertheless, this proved to be enough. Note that not using a line search does not change the validity of the algorithm, but usually more iterations are required to converge. This drawback is approximately offset by the fact that one iteration is much faster without the line search.

5.2.4 Newton's algorithm and its descendants

The conjugate gradient algorithm is quite efficient and for very large scale problems, its memory needs are not significantly worse than those of the gradient method. If, however, there is enough computer memory available, there is – at least theoretically – an even more efficient family of algorithms, called quasi-Newton algorithms. Newton algorithms exist as well, but their efficiency is severely limited by the requirement of computing (and inverting) the Hessian matrix of the system. Let $\mathcal{H}$ denote the Hessian matrix, which is here computed with respect to the fields at all points, i.e. $\mathcal{H} = (h_{\hat{x}\hat{y}})$ and $h_{\hat{x}\hat{y}} = \frac{\partial^2 E}{\partial\phi(\hat{x})\partial\phi(\hat{y})}$ when $\hat{x}, \hat{y}$ enumerate the lattice points. The quasi-Newton methods are all derived from Newton's method, but avoid the time consuming computation of the Hessian and its inversion by building an approximation to the inverse as the iteration proceeds. Generally, these methods require even less iterations than conjugate gradient methods, but there is no guarantee that they are faster in time. The initial value of the inverse Hessian is required to be symmetric and the updates are required to maintain this property. A common choice for the initial value is $\mathcal{H}_0 = \mathrm{Id}$.

Let $\mathcal{H}_k$ denote the approximate inverse Hessian. Then a general quasi-Newton algorithm can be described as follows.

1: $k \leftarrow 0$
2: $d_0 \leftarrow -\nabla E(\Phi_0)$
3: $\mathcal{H}_0 = \mathrm{Id}$
4: **while** not converged **do**
5: perform line search to find λ_k, which minimises $E(\Phi_k + d_k\lambda_k)$
6: $\Phi_{k+1} \leftarrow \Phi_k + \lambda_k d_k$
7: compute $\mathcal{H}_{k+1}$ according to the chosen scheme
8: $d_{k+1} \leftarrow -\mathcal{H}_{k+1}\nabla E(\Phi_{k+1})$

9: $k \leftarrow k + 1$
10: **end while**

The quasi-Newton implementation used here is called the limited memory, variable metric BFGS algorithm which is due to Broyden [79], Fletcher [80], Goldfarb [81] and Shanno [82]. It has some interesting properties solely due to the way the approximate Hessian is updated; for details, see [75]. The BFGS method of updating the inverse Hessian matrix is

$$\delta = \Phi_{k+1} - \Phi_k \tag{5.10}$$

$$\gamma = \nabla E(\Phi_{k+1}) - \nabla E(\Phi_k) \tag{5.11}$$

$$\mathcal{H}_{k+1} = \mathcal{H}_k + \left(1 + \frac{\gamma^T \mathcal{H}_k \gamma}{\delta^T \gamma}\right) \frac{\delta \delta^T}{\delta^T \gamma} - \frac{\delta \mathcal{H}_k \gamma^T + \mathcal{H}_k \gamma \delta^T}{\delta^T \gamma}. \tag{5.12}$$

One interesting property of this formula is the variable metric property, indicated in the name of the algorithm. It is used to describe a situation where the estimated Hessian is guaranteed to be positive definite, hence ensuring that the search direction is indeed towards the minimum. Methods without this property must resort to checking for positive definiteness of the approximated Hessian and use some other direction whenever it is not positive definite; the usual solution is to restart the method with gradient direction, but other solutions exist. For details and proof of the variable metric property, see [75].

The implementation of this algorithm used in [32, 33] has also been derived from the GNU Scientific Library, version 1.9 [78]. It is now known to include a badly designed line search algorithm, so it should not come as a surprise that it is not very efficient. This was, however, not noticed until after most of this work was complete.

It is worth noting that the gradient based methods mentioned above all have equivalent conditions on convergence, the main differences are the number of iterations required, the time elapsed and the amount of computer memory required. The number of iterations is very important in mathematical comparisons of convergence, but in practice, the important factors in deciding which algorithm to use are the time it takes for the algorithm to converge and the amount of memory it requires. It is generally held that the BFGS method is the fastest in elapsed time and the steepest descents is the slowest, but it was noted during this work that it is not always the case. The badly designed line search of GNU Scientific Library

version 1.9 explains, at least in part, why the BFGS was not performing as expected. The exact reasons for the varying performances of the various algorithms are outside the scope of this work. The particular method for each computer run in [32, 33] was selected mostly by the available memory: most of the computations were made using the conjugate gradient algorithm (Fletcher-Reeves scheme), but the steepest descents was used when necessary. Before the poor performance of the implementation of the BFGS algorithm was noticed, it was used whenever memory requirements allowed with the expectation that it would be the fastest. Afterwards, it was only used for several verifications of the results gained by the other algorithms.

5.2.5 Simulated annealing

The simulated annealing algorithm, like the name suggests, mimics a cooling physical process. It was first described by Kirkpatrick el al. and Cerny [83, 84]. It is a type of Metropolis Monte Carlo algorithm by nature, and in some fields of research it is almost always so called instead of simulated annealing. The method itself is very simple: take an initial configuration and make some random changes to it, always accepting a configuration with lower objective value, but also accepting ones with higher values with some probability. The probability depends on a quantity usually called temperature. The probability is the highest when the temperature is the highest. After taking a number of steps at one temperature, it is lowered, and then the process continues. This is repeated until a desired final temperature is reached. Details on how the system is cooled down (called the cooling schedule) and the random number distributions vary, but they do not alter the characteristics of the algorithm.

The most important feature of the simulated annealing algorithm is that it can escape from local minima. Another very important feature is its good suitability to problems which are known to be very hard to solve by other methods. On the other hand, its statistic nature makes it very slow.

A simple version of the algorithm can be described as follows. Let T_0 and T_f be the initial and final temperatures, respectively, and Φ_0 the initial configuration. In the pseudocode $P()$ denotes a probability distribution and $R()$ is a function generating a random number (using some distribution) from the interval $[0, 1)$.

1: $T \leftarrow T_0$
2: $\Phi_{best} \leftarrow \Phi_0$

3: $E_c, E_{best} \leftarrow E(\Phi_0)$
4: **while** $T > T_f$ **do**
5: generate new Φ
6: **if** $E(\Phi) < E_{best}$ **then**
7: $\Phi_{best} \leftarrow \Phi$, $E_{best} \leftarrow E(\Phi)$
8: **end if**
9: **if** $P(E(\Phi), E_c, T, T_f) > R$ **then**
10: $\Phi_0 \leftarrow \Phi$, $E_c \leftarrow E(\Phi)$
11: **end if**
12: reduce T according to the cooling schedule (may result in no change)
13: **end while**

It is usual for $P(a, b, c, d)$ to be such that for $a < b \Rightarrow P(a, b, c, d) = 1$, thus guaranteeing a step whenever it produces a lower objective function value.

The simulated annealing method has been used successfully in the study of topological solitons, for example in [85, 86], but its excessive slowness ruled it out from this work. Some trials were made, however, establishing its applicability. In this work, two implementations of the algorithm have been used. One was an independent implementation and a member of a special class of simulated annealing algorithms, called quench algorithms, where the cooling schedule is trivial: the system is cooled by the same amount at every iteration. This was used in [30, 31]. The other was an adaptation of the one found in GNU Scientific Library and was used in [33].

5.3 Numerical considerations

Section 5.1 introduced the concept of space discretisation, which is necessary in order to use numerical methods like those in Section 5.2. In principle, the algorithms themselves do not introduce errors into the solutions: the error of the result is dictated by the discretisation, not the algorithm. In practice, however, it is generally not possible to find a configuration, where the gradient is exactly zero, even assuming that the discretisation and algorithm themselves are capable of finding it. This is the consequence of the floating point arithmetic of modern computers.

5.3.1 Floating point inaccuracies

Modern computers represent non-integer numbers as approximations. The representation consists of an ordinary base-2 representation, except that

for non-integers negative powers of 2 are included. The number of consecutive powers of two used in the approximation varies; the precision of the current standard format is 16 significant digits, needing 53 bits (representing successive powers of two). In addition there is an exponent of 11 bits and a sign bit. This amount of accuracy is usually good enough for many computational purposes and it is quite sufficient for the work at hand.

Most problems usually come from adding or subtracting numbers of very different magnitude. The energy computation routines used in this work necessarily fall into this category: when summing the energies of different lattice points, eventually the sum will be much larger than the term being added, especially near the boundary of the lattice which is nearly vacuum. For an existence proof this does not matter, however, since these errors do not build up during successive iterations.

The finite precision does affect the convergence, however. Most of the computations presented here were finished before the initially set convergence criterion was satisfied because numerical accuracy was not high enough. This happens when the energy is very close to its minimum and the acceptable step size is very small. In this situation, the values of the field variables are of the order of one and the value of the step size multiplied by the search direction vector is very small. Converging the line search becomes impossible and the minimisation must be stopped. Luckily, this happens only when the gradient is already very small. In this work this happens when the average value of the gradient is of the order of 10^{-7}, and the maximum value of the order of 10^{-2}. Setting a somewhat less stringent convergence criterion (the criterion used here was that the average gradient is $< 10^{-9}$) would have masked the whole effect by stopping the minimisation earlier.

5.3.2 Finite size truncation, finite lattice constant

Another source of error in a numerical investigation comes from finite size effects. Recall that the discretised energy density is only accurate to $\mathcal{O}(h)$. While it can in principle be constructed to be accurate to arbitrary order, $\mathcal{O}(h^n)$, it is rarely practical to any orders $n > 4$. These inaccuracies can be limited by lowering h, but at some point the floating point inaccuracies will be of the same order as the discretisation error, so any further decrease in h will be useless. The point at which this happens is highly problem dependent and it has not been investigated. Usually, floating point inaccu-

racies start to dominate only after $h \lesssim 10^{-5}$, so this is not a likely concern with the values of $h \geq 10^{-2}$ used in this work.

Another obvious source is the finite size L of the computational lattice, supposedly representing an infinite space. The error caused by this truncation is highly dependent on the size of the soliton in the lattice and not related to the lattice spacing in any obvious way. It was noticed during the computations reported in [31] that the finite size cutoff effects can even alter the shape of the core of the minimal energy soliton! For this reason, it has been customary in this work to always check any final configuration in a lattice with roughly doubled size. For an acceptable result the energy should not alter more than what could be expected from the discretisation errors. The virial theorem 2.8 provides a useful check, too.

The finite size of h also means that it is impossible to investigate features smaller in size than h. Usually this is not a concern, since h can be chosen small enough, but in [32] the collapse of the solitonic configuration presented a serious concern. The collapsing soliton would always shrink to a size smaller than h, causing the minimisation algorithm to take "forbidden" steps, steps which are not approximations of any continuous deformation and hence threw the system to another homotopy class, the trivial one. It is not easy to distinguish this purely numerical behaviour from an incorrect implementation of the numerical scheme.

The relative sizes of these sources of error seem to be such that the finite size cutoff effect is the largest, the finiteness of h next, with the floating point errors the smallest by several orders of magnitude. The two largest errors were estimated by both increasing the lattice size L, while keeping h constant and vice versa. The errors were usually of the same order, less than $\mathcal{O}(h)$, except for cases where the shape of the soliton was affected by the boundary. After ensuring the soliton is in a large enough lattice, the cutoff error falls below the finiteness error. The size of the floating point error was estimated for some of the computations by making the same computations in both 32 and 64 bit floating point arithmetic; the results were identical to within 6 significant digits. This can be considered very good because this is one less than the maximum number of accurate digits in 32 bit floating point numbers.

5.3.3 On convergence

In mathematical treatments of optimisation algorithms, exact values for all variables are often assumed. In that situation, the gradient based algorithms converge when the gradient is zero, and some rigorous results can be obtained, like the one mentioned in Section 5.2.3. As was seen in Section 5.3, in computer implementations, the inaccuracies explained in Sections 5.3.1 and 5.3.2 creep into the system in addition to the floating point numbers being inherently approximative. Indeed, it was explained in Section 5.3.1 how the floating point inaccuracy sometimes prevents the algorithm from achieving the desired precision.

The simulated annealing algorithm does not have a proper concept of convergence: it simply reaches the desired temperature and stops. For many systems, the function changes less and less when this temperature is approached, but this is not always the case. Therefore, the method is most often employed not to find the minimum of the objective function, but a small enough value. In some situations, the local minima may be very close to the global minimum and requiring that the shortest route is found may increase the necessary computing time disproportionately.

Chapter 6

Results

This chapter summarises the results of this research, grouped according to the model.

6.1 The Faddeev-Skyrme model

Hopfions of the Faddeev-Skyrme model were studied in [30], [31] and [34]. Although the model is the same in all three articles, the boundary conditions used were different. As was seen in Chapter 3, imposing the boundary conditions modifies the topological character of the system. This section is divided according to the boundary conditions of the field on the domain.

6.1.1 Domain homeomorphic to S^3

The work done in [30] is a direct continuation of [62, 63] and the same boundary condition

$$\lim_{\|x\|\to\infty} \Phi(x) \to \Phi(\infty) \tag{6.1}$$

was used. This compactifies the domain to S^3 and the relevant topological invariant is the Hopf invariant. This work presents a detailed investigation of the processes involved when the preimages of the initial configuration deform into the final ones. Especially interesting is the case where a set of preimages becomes a single preimage or vice versa.

These processes conserve the Hopf invariant and should therefore be possible in any system with Hopfions. At the core of these deformations is the splitting and reconnection of preimages. Recall from Section 3.5.3 that the preimage of a point, $\Phi^{-1}(x)$, is either a single loop or a set of loops. Let

$N_\Phi(x)$ be the number of distinct loops in the preimage $\Phi^{-1}(x)$. Suppose then that there is a configuration and points x, y such that $N_\Phi(x) < N_\Phi(y)$. By continuity there are then $N_\Phi(y) - N_\Phi(x)$ points z_i, $i \in [1, N_\Phi(y) - N_\Phi(x)]$ for which $N_\Phi(z_i) = N_\Phi(x) + i$, and whose preimages interpolate between the preimages $\Phi^{-1}(x)$ and $\Phi^{-1}(y)$. Furthermore, this interpolation is such that for each z_i, some two of the previously distinct loops share a single point. This process, when viewed from $\Phi^{-1}(x)$ to $\Phi^{-1}(y)$, is the splitting of preimages and the other direction is the reconnection. An example of this process is shown in Figure 6.1, where a formation of a figure-8 loop is displayed. Each colour represents a single preimage and the sequence of four colours represents a preimage of a line segment.

Again, by continuity, it is impossible to change the linking number of preimages in this process. Also, it is unknown whether three or more preimages can simultaneously reconnect or split, that is, if three or more previously distinct loops can share a single point. From topological arguments, this may be possible, but to date there seems to be no observation of such process. The reason may be that such a process is energetically unfavourable.

6.1.2 Partially periodic domain, $\mathsf{S}^2 \times \mathsf{S}^1$

In [31] the boundary conditions are different as follows. Let $(x_i)_\pm$ be the minimum and maximum values of x_i coordinate within the lattice and $L = (x_3)_+ - (x_3)_-$. Then the boundary conditions can be written as

$$\begin{cases} \Phi\big((x_1)_\pm, x_2, x_3\big) = \Phi\big(x_1, (x_2)_\pm, x_3\big) = (0,0,1)^T \\ \Phi\big(x_1, x_2, x_3\big) = \Phi\big(x_1, x_2, x_3 + L\big). \end{cases} \tag{6.2}$$

The initial configuration is now a vortex in the periodic direction. The boundary conditions change the domain to $\mathsf{S}^2 \times \mathsf{S}^1$, which invalidates the one-point compactification of $\mathbb{R}^3 \to \mathsf{S}^3$ but, as was noted in Section 4.1.2, the linking number of preimages is still well defined and will now be called the Hopf invariant, too. The energy of the vortex is finite per unit length.

The main result of [31] was the identification of minimum energy configurations for vortices with conserved Hopf invariants $H \in [5, 8]$. Recall from Section 3.5.2, that the Hopf invariant is not necessarily conserved in this case. The real homotopy invariants are the Pontrjagin invariants s_1 and s_2; for all the computations of [31], the value $s_2 = 1$ was used. The

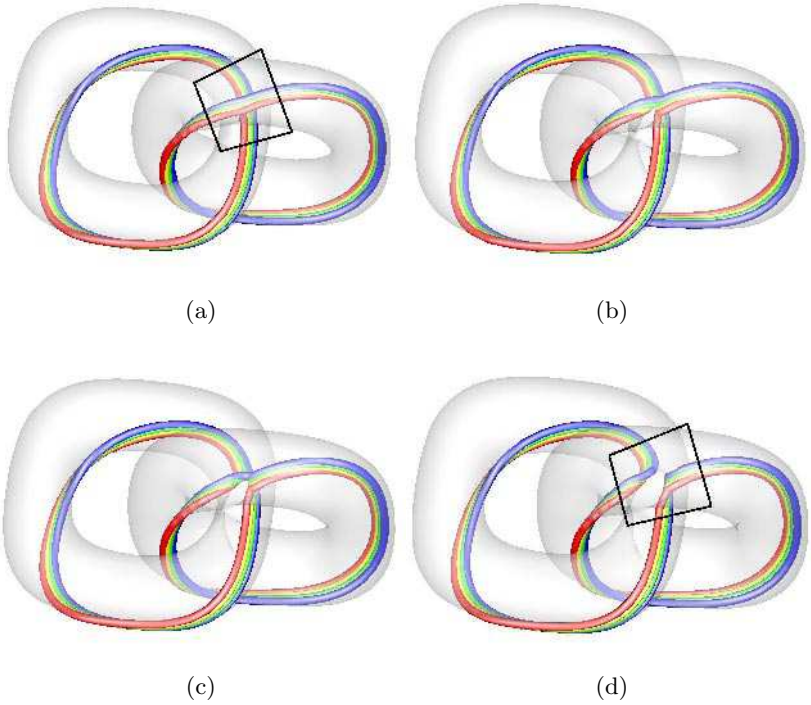

(a) (b)

(c) (d)

Figure 6.1: A sequence of images (a)-(d) showing the splitting-reconnecting process of a two linked loops into a single figure-8 loop. Each colour represents one preimage and the sequence of four colours represents a preimage of a line segment. The figures are reproduced from [30].

value of s_1 was not considered.

It was found that the resulting configurations have the following resemblance to the closed knot-like Hopfions of the usual Faddeev-Skyrme system: if the core of a closed Hopfion is cut at one point and resulting ends pulled to the edges of the lattice, the result looks just like the minimum energy configuration of the vortex system. This is shown in Figure 6.2, where the initial and final configurations of knot and vortex Hopfions of $H = 7$ are shown beside the corresponding minimum energy configurations.

Another intriguing discovery in [31] was the indication that the lower bound of the energy of the vortices might be a linear function of the Hopf

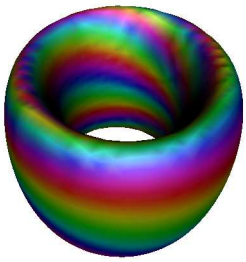

(a) Initial state of the knot Hopfion

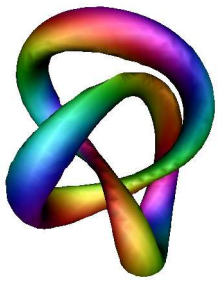

(b) Final state of the knot Hopfion

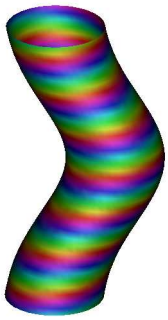

(c) Initial state of the vortex Hopfion

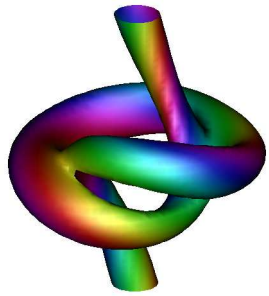

(d) Final state of the vortex Hopfion

Figure 6.2: Comparison of knot and vortex Hopfions of $H = 7$.

invariant, $E > 130.72 + 75.312\,|H|$, instead of the $E \sim H^{3/4}$ of the closed Hopfions studied earlier. The form of the energy bound for these systems is still an open question [87].

6.1.3 Fully periodic domain, $\mathbf{T^3}$

The altered boundary conditions were taken a step further in [34]. The boundaries are periodic for all dimensions:

$$\Phi\big(x\big) = \Phi\big(x + L\hat{e}_j\big) \quad \forall\, j \in \{1, 2, 3\}. \tag{6.3}$$

The initial configurations were sets of identical vortices packed closely together and the individual vortices were the same as in [31].

Earlier studies had concentrated in single vortices (and single or double knot-like Hopfions), but there are many systems, where bunches of vortices form; e.g. liquid helium [39, 22, 23].

The condition 6.3 further alters the topology of the system: the domain is now topologically T^3, the 3-torus.[1] Now that restriction has been relaxed as much as possible while keeping the domain T^3. The homotopy classification is given by theorem 3.18 and even though these integers do not provide a complete classification of the maps, they are homotopy invariants. Hence, even tough the Hopf invariant is no longer useful, there is still possibility of topological solitons, classified by the invariants t_i introduced in Section 3.5.2.

Indeed, it was observed in [34] how the linking number of preimages can vanish in a continuous deformation driven by energy minimisation, while the real homotopy invariants t_i are conserved. Vanishing follows after repeated preimage splittings and reconnections across the xy-boundary and the final configuration consists of only straight preimages in the z-direction with no linking. These splittings and reconnections follow the same rules as those reported in [30, 31].

By putting a set of four vortices in a lattice whose dimensions were large compared to the volume occupied by the vortices [34], the behaviour was altered. As expected, the energy minimisation process now favours configurations where the non-trivial sections of the configuration do not approach the xy-boundaries and hence reconnections and splittings across the boundary cannot occur, while they still occur between neighbouring vortices. The final configuration is a bunch of intertwined vortices with the Hopf invariant and the real homotopy invariants t_i conserved. One intermediate state and the final configuration are shown in Figure 6.3, where the preimages of $(0, 0, -1)$ (blue) and a point with $n_3 = 0.1$ (red) are displayed. By counting the linking number of preimages it can be seen that the initial linking number of 24 has been conserved while the initially separate, straight vortices have deformed to a bunch of intertwined vortices.

Thus the Hopf invariant is conserved even though it is not a homotopy invariant in this system. The behaviour of the system here is similar to

[1] From the point of view of the computational lattice, it could be argued that even the domain of the knot-like closed vortices was T^3, albeit with the value of Φ fixed to $(0, 0, 1)^T$ in some region.

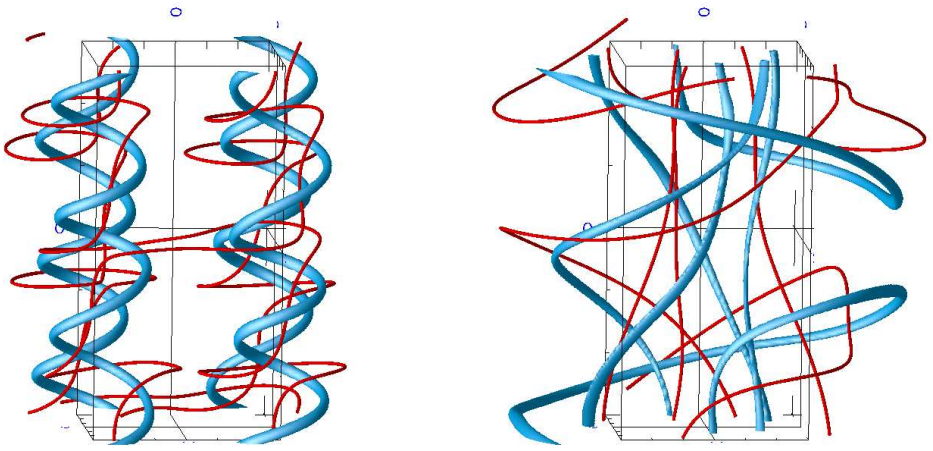

(a) (b)

Figure 6.3: An intermediate (a) and final (b) configuration of a set of four identical parallel vortices. The preimages of the core (blue) and one point from $n_3 = 0.1$ (red) are shown; the wire frame shows the size of the lattice in z-direction and locations of the cores of the initial configuration. The computational box is larger and the thicknesses of the tubes are arbitrary.

the case where the domain is $\mathsf{S}^2 \times \mathsf{S}^1$, where the Hopf invariant is also conserved even though it is not a homotopy invariant there either. The same is believed to hold for a closed Hopfion as well, so in T^3, the knot soliton is stable only if the T^3 is large enough.

6.2 Ginzburg-Landau model

It was noted in Section 4.2.2 that there are no non-zero global minima in the homotopy classes of $\chi = \Psi/\|\Psi\|$ in the Ginzburg-Landau model. However, in [88] one possible local minimum is identified, but that has not been confirmed. Thus, it remains an open question whether there are local minima and what the corresponding field configurations might look like.

To answer this, an extensive search, spanning much of the parameter space of the model was performed in [32]. No non-zero minima were found, but the relaxation process always, after some initial buildup of magnetic field energy, leads to a vanishing magnetic field energy accompanied by simultaneous shrinking of the core of the toroidal soliton. In a continuum model, this shrinkage could eventually lead to a core, whose radius approaches zero until it is much smaller than the lattice spacing. This happens even with the smallest lattice spacings that were computationally possible. This concentrates all the energy density to a curve with zero integrated total energy. The topology is still unchanged: the shrinkage is simply a homotopy where the radius r of the core is reduced by a homotopy $h(t) = (t-1)r$ with the final value of t arbitrarily close to unity. The picture in the numerical investigation is drastically different. Recall from Section 5.3.2 that it is not possible to investigate features smaller than the lattice spacing. Now, the homotopy h will inevitably shrink the soliton into sizes smaller than the lattice spacing no matter how small the lattice spacing is.

The relaxation process, however, yields a surprise: the shrinkage of the soliton is accompanied not only by decreasing magnetic energy, but also by decreasing $\|\Psi\|$ at some point. This is unfortunate, because the moment there is even a single point in the lattice where $\|\Psi\| = 0$, the compactification $\mathbb{R}^3 \to \mathsf{S}^3$ of the configuration space fails, giving a map $\mathsf{S}^3 \to \mathbb{R}^3$. Since $\pi_3(\mathbb{R}^3) = 0$, these maps are uninteresting. Even if at a later point in the relaxation $\|\Psi\| > 0$ everywhere again, there is no reason to hope that the homotopy class of χ obtained from this Ψ would be the same as before the moment when $\|\Psi\| = 0$. Indeed, it was observed that

even though the potential term $V(\Psi) = c(\|\Psi\|^2 - 2)^2$ yields an increasing energy when $\|\Psi\| \to 0$, there is a point in the relaxation process where $\|\Psi\| = 0$ somewhere in the lattice. The numerical approximation of $\deg \Psi$ falls to zero simultaneously, thus confirming that the topology has changed at the moment when $\|\Psi\| = 0$ somewhere.

Therefore, it was necessary prevent Ψ from vanishing. Increasing the above potential strength c by several orders of magnitude did not change the process (numerical inaccuracies place an upper limit on possible values of c), so something else was needed. The potential was altered to include a term of the form $b/\|\Psi\|^2$ in the hope that it would increase fast enough to stop the vanishing of $\|\Psi\|$. Now it was possible to follow the decrease of magnetic field without associated vanishing of $\|\Psi\|$ and the result was a confirmation that the vanishing magnetic field allows homotoping the dimensions of the soliton into sizes smaller than the lattice spacing. Thus none of the initial configurations and parameters investigated in [32] lead to a non-zero local minimum under an energy minimisation process. However, it cannot be ruled out that there are some well hidden local minima which need an initial configuration very close to the minimum in order to be found.

6.3 Ward's modification of the Ginzburg-Landau model

The search for local minima of the Ginzburg-Landau model is not yet over. Ward showed [73] that by modifying the energy density by adding the term (4.26) and using the potential (4.27), local minima can be found on the curve $\eta = \kappa^2 + 1$ of the parameter space. This work was expanded in [33] to the $\eta\kappa$-plane of the parameter space (the parameter space is actually three dimensional). The main results of [33] were the shape of the boundary between the regions of parameter space yielding stable solitons and unstable ones, and the energy of the solitons along this boundary. Figure 6.4a shows the approximate shape of the boundary with stable configurations above and to the right of the curve and unstable ones below and to the left. Figure 6.4b yields an intriguing result: the energy along the above boundary does not change, even though the size of the minimum energy soliton is different along the boundary. These results may be of assistance in any future attempts to construct an initial configuration which yields a non-zero local minimum.

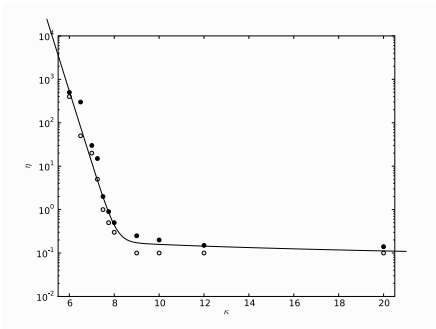

(a) Boundary between stable and unstable regions: the solid black circles denote pairs of (κ, η_κ), yellow circles denote the largest unstable values of η and the curve, $\eta = 45^{7.65-\kappa} + 0.5\kappa^{-\frac{1}{2}}$ approximates the boundary.

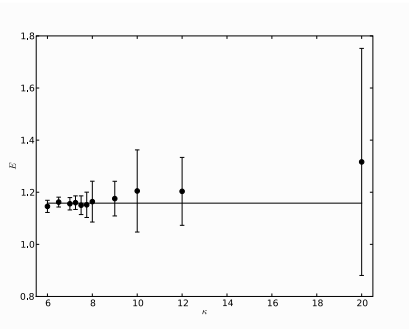

(b) Energies (black discs) of the stable configurations closest to the boundary, the heights of the error bars show the inaccuracy of the solution as determined from the virial theorem and the horizontal line is the least-squares fit of a constant energy.

Figure 6.4: The boundary between stable and unstable regions (a) and the energies of stable configurations closest to the boundary (b). The figure is reproduced from [33].

Ultimately, investigations of this modification of the Ginzburg-Landau model, and possibly other modifications as well, may provide such insight into the model that it is possible to construct an initial configuration which yields a non-zero local minimum in the plain Ginzburg-Landau model. Of course, it is quite possible that such minima do not exist, but it seems unlikely to rule out their existence with numerical investigations only; a rigorous proof would most likely be necessary to establish their non-existence. Meanwhile, some of these modifications, like that of [72], may turn out to be physically relevant in addition to just providing insight into the structure of the minima of the Ginzburg-Landau energy functional.

Chapter 7

Conclusions

This work consists of a number of original research results regarding the Faddeev-Skyrme model [30], [31], [34] and Ginzburg-Landau model [32], [33]. In the Faddeev-Skyrme model, unconventional boundary values have been imposed, resulting in topologically slightly different models than the usual one, but nevertheless possessing topological invariants and a rich variety of phenomena related to the topological solitons of the model. In [31], where the field is $\Phi : \mathsf{S}^2 \times \mathsf{S}^1 \to \mathsf{S}^2$, sliced and straightened versions of the familiar knot solitons are encountered as minimum energy configurations and in [30] the processes of preimage splitting and reconnection are shown to be the dominant method of deformation in many situations.

In [34], a version of the model where $\Phi : \mathsf{T}^3 \to \mathsf{S}^2$ was studied. The model now has a different topological classification due to Pontrjagin [45] and a very different picture emerges, involving unwinding the usual twisted structure, but nevertheless having the necessary features to warrant being called a topological soliton. The familiar preimage splitting and reconnection processes are responsible for the unwinding.

The two component Ginzburg-Landau model was investigated in [32] and despite extensive searching, no non-trivial local minima were found. This does not form a proof of their non-existence, but does provide a strong argument against their existence within the region of the parameter space investigated. The processes leading to the trivial minimum were carefully analysed, revealing that there are two possible outcomes. The first one is the expected shrinking of the soliton due to a vanishing magnetic field, but the second involves a violation of the assumption $\|\Psi\| > 0$ everywhere, which is the requirement for the existence of topologically non-trivial configurations. Violating this assumption is both physically and mathematically valid, but it has the unfortunate side-effect of producing a configuration

which is no longer a map $\Psi : \mathsf{S}^3 \to \mathsf{S}^3$ but instead $\Psi : \mathsf{S}^3 \to \mathbb{R}^3$, where the topology is trivial and the topological information of the initial configuration is lost.

Local minima with non-zero energy were found to exist in an extended Ginzburg-Landau model studied in [33]. These take the familiar shape of the (un-)knot Hopfion. A certain two-dimensional subset of the three dimensional parameter space was divided into two regions, according to whether local minima with non-zero energy exist or not. The approximate shapes of these regions were found. Perhaps the most interesting result was that the energy of the stable Hopfion on the boundary between these regions seems constant.

The results obtained in this work shed light on the properties of the Ginzburg-Landau model, perhaps helping in delivering the final judgement on the existence of its non-trivial local minima. The Ginzburg-Landau model is a well established model of superconductors and -fluids, and therefore theoretical understanding of the model is important for our understanding of these important phenomena in nature.

The results of the Faddeev-Skyrme and Ginzburg-Landau models provide insight into the general processes and properties of Hopfions and the models themselves, in addition to widening our understanding of how these models can be used as building blocks in understanding features of effective field theories, which may play an important part in areas like quark confinement [14, 28]. Other theoretical models related to Hopfions include three dimensional ferromagnets [17], electrically conducting plasmas [89], and topological insulators [90].

The Faddeev-Skyrme and Ginzburg-Landau models are also related to such experimentally observed phenomena as vortex solitons in superfluid helium [16, 91, 24], the Abrikosov vortices of superconductors [4], non-Meissner superconductors [25] and possibly even topological insulators [26].

Appendix A

Notation

The following notations and conventions are used in this work unless otherwise stated. The usual notations of theoretical physics, such as the Einstein summation convention are used throughout and the metric $g_{\mu\nu}$ is always such that $g_{00} = 1$ and $g_{jj} = -1$ for $j > 0$.

$\mathcal{P}$	Physical space, domain of the field maps.
$\mathcal{C}$	Configuration space, target of the field maps.
D	Dimension of physical space without time; $D = \dim \mathcal{P} - 1$.
$\hat{e}_j$	jth basis unit-vector of the physical space.
x^j	jth coordinate of $\mathcal{P}$; $x_j = g_{jk}x^k$. Also time $t = x^0$.
x	$D+1$-dimensional vector (or $1\times(D+1)$-matrix) $(x_0, x_1, \ldots, x_D)$.
Φ	Always denotes a map $\Phi : \mathcal{P} \to \mathcal{C}$.
ϕ_j	jth component of Φ.
∂_j	$\partial_j \equiv \frac{\partial}{\partial x^j}$.
∇	For a function f this is the vector $\nabla f = (\partial_1 f, \ldots, \partial_D f)$.
	For a vector f this is the matrix $\left(\nabla f\right)_{jk} = \partial_j f_k$.
∇_Φ	For a discretised Φ, ∇_Φ denotes the derivatives with respect to all fields Φ at all lattice points.
∂	For a function or vector f, $\partial f \equiv (\partial_0 f, \nabla f)$.
	For a space or set X, ∂X is the boundary of X.
$\mathcal{L}$	Lagrangian density $\mathcal{L} = \mathcal{L}(f, \partial f)$.
$\mathcal{E}$	Energy density of the corresponding Lagrangian density.
E	Total energy, $E = \int_{\mathcal{P}} \mathcal{E}$.

$\Re$, $\Im$	Real and imaginary parts, respectively, of a complex number.
$\bar{z}$	Complex conjugate of z.
z^T	Transpose of z.
$z^\dagger$	Adjoint of z, $z = \bar{z}^T$.
Id	Identity matrix.
$\mathbb{N}$	The set of natural numbers, *not including zero*, i.e. $\mathbb{N} \equiv \{1, 2, ...\}$.
$f\|U$	Restriction of function $f : X \to Y$ to $U \subset X$.
$f(\infty)$	$f(\infty) \equiv \lim_{\|x\|\to\infty} f(x)$.
$\epsilon_{i_1 \ldots i_n}$	Totally antisymmetric permutation symbol: changing any two indices changes the sign. If the indices form an increasing sequence, $\epsilon_{\text{indices}} = 1$.
$\|f\|$	For an f with one index, this is the usual norm $\|f\| \equiv \sqrt{\sum_j (f_j^2)}$. For f with two indices, this is the Hilbert-Schmidt norm $\|f\| \equiv \sqrt{\sum_{jk} (\|f_{jk}\|^2)}$.
S^n	n-dimensional sphere, $\mathsf{S}^n \equiv \{x \in \mathbb{R}^{n+1} \big\| \|x\| = 1\}$.
D^n	n-dimensional ball, $\mathsf{D}^n \equiv \{x \in \mathbb{R}^n \big\| \|x\| \leq 1\}$.
H	The map giving the Hopf invariant; sometimes also the value of h when applied to some function.

Bibliography

[1] W. H. Thomson, "On vortex atoms," *Proc. Roy. Soc. Edin.* **6** (1867) 94–105.

[2] P. A. M. Dirac, "Quantised singularities in the electromagnetic field," *Proc. Roy. Soc. Lond.* **A133** (1931) 60–72.

[3] P. A. M. Dirac, "The theory of magnetic poles," *Phys. Rev.* **74** (1948) 817–830.

[4] A. A. Abrikosov, "On the Magnetic properties of superconductors of the second group," *Sov. Phys. JETP* **5** (1957) 1174–1182.

[5] T. H. R. Skyrme, "A nonlinear theory of strong interactions," *Proc. Roy. Soc. A* **247** (1958) 260.

[6] T. H. R. Skyrme, "A unified model of k and pi mesons," *Proc. Roy. Soc. A* **252** (1959) 236.

[7] T. H. R. Skyrme, "A non-linear field theory," *Proc. Roy. Soc. A* **260** (1961) 127.

[8] T. H. R. Skyrme, "A unified field theory of mesons and baryons," *Nucl. Phys.* **31** (1962) 556.

[9] G. 't Hooft, "Magnetic monopoles in unified gauge theories," *Nucl. Phys.* **B79** (1974) 276–284.

[10] A. M. Polyakov, "Particle spectrum in quantum field theory," *JETP Lett.* **20** (1974) 194–195.

[11] B. Julia and A. Zee, "Poles with both magnetic and electric charges in nonabelian gauge theory," *Phys. Rev.* **D11** (1975) 2227–2232.

[12] L. D. Faddeev, "Quantization of Solitons,". pre-print-75-0570 (IAS, PRINCETON).

[13] T. W. B. Kibble, "Topology of cosmic domains and strings," *J. Phys.* **A9** (1976) 1387–1398.

[14] L. D. Faddeev and A. J. Niemi, "Partially dual variables in SU(2) Yang-Mills theory," *Phys. Rev. Lett.* **82** (1999) 1624–1627, `hep-th/9807069`.

[15] M. Kléman, "Defects in liquid crystals," *Rept. Prog. Phys.* **52** (1989) 555–654.

[16] V. M. H. Ruutu, U. Parts, J. H. Koivuniemi, M. Krusius, E. V. Thuneberg, and V. G. E., "The intersection of a vortex line with a transverse soliton plane in rotating 3He-A: Pi3 topology," *JETP Lett.* **60** (1994) 671.

[17] T. A. Ioannidou and P. M. Sutcliffe, "Soliton dynamics in 3D ferromagnets," *Physica* **D150** (2001) 118–126, `cond-mat/0101129`.

[18] E. Witten and D. Olive, "Supersymmetry algebras that include topological charges," *Physics Letters B* **78** (1978) 97 – 101.

[19] M. J. Bowick, L. Chandar, E. A. Schiff, and A. M. Srivastava, "The cosmological Kibble mechanism in the laboratory: String formation in liquid crystals," *Science* **263** (1994) 943–945, `hep-ph/9208233`.

[20] U. Essmann and H. Träuble, "The direct observation of individual flux lines in type II superconductors," *Physics Letters A* **24** (1967) 526 – 527.

[21] M. R. Matthews, B. P. Anderson, P. C. Haljan, D. S. Hall, C. E. Wieman, and E. A. Cornell, "Vortices in a Bose-Einstein condensate," *Phys. Rev. Lett.* **83** (1999) 2498–2501.

[22] V. M. H. Ruutu, V. B. Eltsov, A. J. Gill, T. W. B. Kibble, M. Krusius, Y. G. Makhlin, B. Placais, G. E. Volovik, and W. Xu, "Big bang simulation in superfluid 3He-B – vortex nucleation in neutron-irradiated superflow," *Nature* **382** (1996) 334, `cond-mat/9512117`.

[23] C. Bäuerle, Y. M. Bunkov, S. N. Fisher, H. Godfrin, and G. R. Pickett, "Laboratory simulation of cosmic string formation in the early Universe using superfluid ^{3}He," *Nature* **382** (1996) 332.

[24] T. D. C. Bevan, A. J. Manninen, J. B. Cook, J. R. Hook, H. E. Hall, T. Vachaspati, and G. E. Volovik, "Momentum creation by vortices in superfluid ^{3}He as a model of primordial baryogenesis," *Nature* **386** (1997) 689.

[25] V. V. Moshchalkov, M. Menghini, T. Nishio, Q. H. Chen, A. V. Silhanek, V. H. Dao, L. F. Chibotaru, N. D. Zhigadlo, and J. Karpinsky, "Type-1.5 superconductors," *Phys. Rev. Lett* **102** (2009) 117001, `arXiv:0902.0997v3 [cond-mat]`.

[26] D. Hsieh, Y. Xia, L. Wray, D. Qian, A. Pal, J. H. Dil, J. Osterwalder, F. Meier, G. Bihlmayer, C. L. Kane, Y. S. Hor, R. J. Cava, and M. Z. Hasan, "Observation of Unconventional Quantum Spin Textures in Topological Insulators," *Science* **323** (2009) 919–922.

[27] M. Hindmarsh, "Semilocal topological defects," *Nucl. Phys.* **B392** (1993) 461–492, `hep-ph/9206229`.

[28] E. Langmann and A. J. Niemi, "Towards a string representation of infrared SU(2) yang- mills theory," *Phys. Lett.* **B463** (1999) 252–256, `hep-th/9905147`.

[29] E. Babaev, L. D. Faddeev, and A. J. Niemi, "Hidden symmetry and duality in a charged two-condensate Bose system," *Phys. Rev.* **B65** (2002) 100512, `cond-mat/0106152`.

[30] J. Hietarinta, J. Jäykkä, and P. Salo, "Dynamics of vortices and knots in Faddeev's model," in *Workshop on Integrable Theories, Solitons and Duality*. PoS(unesp2002)017 (2002). `http://pos.sissa.it/archive/conferences/008/017/unesp2002_017.pdf`.

[31] J. Hietarinta, J. Jäykkä, and P. Salo, "Relaxation of twisted vortices in the Faddeev-Skyrme model," *Phys. Lett.* **A321** (2004) 324–329, `cond-mat/0309499`.

[32] J. Jäykkä, J. Hietarinta, and P. Salo, "Topologically nontrivial configurations associated with Hopf charges investigated in the two-component Ginzburg-Landau model," *Phys. Rev.* **B77** (2008) 094509, `cond-mat/0608424`.

[33] J. Jäykkä, "Stability of topological solitons in modified two-component Ginzburg-Landau model,"
Phys. Rev. **D79** (2009) 065006, `arXiv:0901.4579 [hep-th]`.

[34] J. Jäykkä and J. Hietarinta, "Unwinding in Hopfion vortex bunches,"
to be published in Phys. Rev. **D** (2009) , `arXiv:0904.1305 [hep-th]`.

[35] Y. Choquet-Bruhat, C. DeWitt-Morette, and M. Dillard-Bleick, *Analysis, Manifolds and Physics*. North Holland, 1992.

[36] G. H. Derrick, "Comments on nonlinear wave equations as models for elementary particles," *J. Math. Phys.* **5** (1964) 1252.

[37] E. B. Bogomolny, "Stability of Classical Solutions," *Sov. J. Nucl. Phys.* **24** (1976) 449.

[38] N. S. Manton and P. Sutcliffe, *Topological solitons*. Cambridge University Press, 2004.

[39] W. H. Zurek, "Cosmological Experiments in Superfluid Helium?," *Nature* **317** (1985) 505–508.

[40] R. Bott and L. W. Tu, *Differential forms in algebraic topology*. Springer-Verlag, 1982.

[41] A. Hatcher, *Algebraic Topology*. Cambridge University Press, 2002.

[42] M. J. Ablowitz, D. J. Kaup, A. C. Newell, and H. Segur, "Method for solving the Sine-Gordon equation,"
Phys. Rev. Lett. **30** (1973) 1262–1264.

[43] H. Flanders, *Differential forms with applications to the physical sciences*. Dover Publications, 1989.

[44] R. H. Fox, "Torus Homotopy Groups," *Proceedings of the National Academy of Science* **31** (1945) 71–74.

[45] L. S. Pontrjagin, "A classification of mappings of the three-dimensional complex into the two-dimensional sphere," *Rec. Math. [Mat. Sbornik] N.S.* **9** (1941) 331–363.
`http://mi.mathnet.ru/eng/msb6073`.

[46] D. Auckly and L. Kapitanski, "Analysis of S^2-valued maps and Faddeev's model," *Comm. Math. Phys.* **256** (2005) 611–620.

[47] T. H. R. Skyrme, "Particle states of a quantized meson field," *Proc. Roy. Soc. A* **262** (1961) 237.

[48] T. H. R. Skyrme, "A model unified field equation," *Nucl. Phys.* **31** (1962) 550.

[49] E. Witten, "Global Aspects of Current Algebra," *Nucl. Phys.* **B223** (1983) 422–432.

[50] E. Witten, "Current Algebra, Baryons, and Quark Confinement," *Nucl. Phys.* **B223** (1983) 433–444.

[51] A. F. Vakulenko and L. V. Kapitanskii, "Stability of solitons in S^2 in the nonlinear σ-model," *Sov. Phys. Dokl.* **24** (1979) 433.

[52] R. S. Ward, "Hopf solitons on S^3 and $\mathbb{R}^3$," *Nonlinearity* **12** (1999) 241–246, `hep-th/9811176`.

[53] A. Kundu and Y. P. Rybakov, "Closed vortex type solitons with Hopf index," *J. Phys.* **A15** (1982) 269–275.

[54] R. A. Battye and P. Sutcliffe, "Solitons, links and knots," *Proc. Roy. Soc. Lond.* **A455** (1999) 4305–4331, `hep-th/9811077`.

[55] H. J. de Vega, "Closed Vortices and the Hopf Index in Classical Field Theory," *Phys. Rev.* **D18** (1978) 2945.

[56] U. Enz, "A New Type of Soliton with Particle Properties," *J. Math. Phys.* **18** (1977) 347–353.

[57] D. A. Nicole, "Solitons with nonvanishing Hopf index," *J. Phys.* **G4** (1978) 1363.

[58] J. Gladikowski and M. Hellmund, "Static solitons with non-zero Hopf number," *Phys. Rev.* **D56** (1997) 5194–5199, `hep-th/9609035`.

[59] L. D. Faddeev and A. J. Niemi, "Knots and particles," *Nature* **387** (1997) 58, `hep-th/9610193`.

[60] L. D. Faddeev and A. J. Niemi, "Toroidal configurations as stable solitons," hep-th/9705176.

[61] R. A. Battye and P. M. Sutcliffe, "Knots as stable soliton solutions in a three-dimensional classical field theory," *Phys. Rev. Lett.* **81** (1998) 4798–4801, hep-th/9808129.

[62] J. Hietarinta and P. Salo, "Faddeev-Hopf knots: Dynamics of linked un-knots," *Phys. Lett.* **B451** (1999) 60–67, hep-th/9811053.

[63] J. Hietarinta and P. Salo, "Ground state in the Faddeev-Skyrme model," *Phys. Rev.* **D62** (2000) 081701(R).

[64] P. Sutcliffe, "Knots in the Skyrme-Faddeev model," *Proc. Roy. Soc. Lond.* **A463** (2007) 3001–3020, arXiv:0705.1468v1 [hep-th].

[65] F. Lin and Y. Yang, "Existence of Energy Minimizers as Stable Knotted Solitons in the Faddeev Model," *Communications in Mathematical Physics* **249** (2004) 273–303.

[66] C. Adam, J. Sanchez-Guillen, R. A. Vazquez, and A. Wereszczynski, "Investigation of the Nicole model," *J. Math. Phys.* **47** (2006) 052302, hep-th/0602152.

[67] M. Hirayama, H. Yamakoshi, and J. Yamashita, "Estimation of the Lin-Yang bound of the least static energy of the Faddeev model," *Prog. Theor. Phys.* **116** (2006) 273–283, hep-th/0602192.

[68] H. Aratyn, L. A. Ferreira, and A. H. Zimerman, "Exact static soliton solutions of 3+1 dimensional integrable theory with nonzero Hopf numbers," *Phys. Rev. Lett.* **83** (1999) 1723–1726, hep-th/9905079.

[69] H. Hopf, "Über die abbildungen der dreidimensionalen Sphäre auf die Kugelfläche," *Mathematische Annalen* **104** (1931) 637–665.

[70] A. Vilenkin and E. P. S. Shellard, *Cosmic Strings and other Topological Defects*. Cambridge University Press, 1994.

[71] J. M. Speight, "Supercurrent coupling in the Faddeev-Skyrme model," arXiv:0812.1493 [hep-th].

[72] E. Babaev, "Non-Meissner electrodynamics and knotted solitons in two-component superconductors," `arXiv:0809.4468v3 [cond-mat]`.

[73] R. S. Ward, "Stabilizing textures with magnetic fields," *Phys. Rev.* **D66** (2002) 041701(R), `hep-th/0207100`.

[74] K. G. Wilson, "Confinement of quarks," *Phys. Rev.* **D10** (1974) 2445–2459.

[75] R. Fletcher, *Practical Methods of Optimization*. Wiley, 1980.

[76] R. Fletcher and C. M. Reeves, "Function minimization by conjugate gradients," *Computer Journal* **7** (1964) 149–154.

[77] E. Polak and G. Ribière, "Note sur la convergence de méthodes de directions conjuguées," *Rev. Françeaise Informat. Recherche Opérationnelle* **3** (1969) 35–43.

[78] Mark Galassi *et al*, *GNU Scientific Library Reference Manual (2nd Ed.)*. Network Theory Limited, 2006. `http://www.gnu.org/software/gsl/`.

[79] C. G. Broyden, "The convergence of a class of double-rank minimization algorithms," *Journal of the Institute of Mathematics and Its Applications* **6** (1970) 76–90.

[80] R. Fletcher, "A new approach to variable metric algorithms," *Computer Journal* **13** (1970) 317–322.

[81] D. Goldfarb, "A family of variable metric updates derived by variational means," *Mathematics of Computation* **24** (1970) 23–26.

[82] D. F. Shanno, "Conditioning of quasi-newton methods for function minimization," *Mathematics of Computation* **24** (1970) 647–656.

[83] S. Kirkpatrick, C. D. Gelatt, and M. P. Vecchi, "Optimization by simulated annealing," *Science* **220** (1983) 671–680.

[84] V. Cerny, "A thermodynamical approach to the travelling salesman problem: an efficient simulation algorithm," *Journal of Optimization Theory and Applications* **45** (1985) 41–51.

[85] M. Hale, O. Schwindt, and T. Weidig, "Simulated annealing for topological solitons," *Phys. Rev.* **E62** (2000) 4333–4346, `hep-th/0002058`.

[86] R. A. Battye, C. J. Houghton, and P. M. Sutcliffe, "Icosahedral Skyrmions," *J. Math. Phys.* **44** (2003) 3543–3554, `hep-th/0210147`.

[87] M. Miettinen, A. J. Niemi, and Y. Stroganov, "Aspects of duality and confining strings," *Phys. Lett.* **B474** (2000) 303–308, `hep-th/9908178`.

[88] A. J. Niemi, K. Palo, and S. Virtanen, "(Meta)stable closed vortices in (3+1)+dimensional gauge theories with an extended Higgs sector," *Phys. Rev.* **D61** (2000) 085020.

[89] L. Faddeev and A. J. Niemi, "Magnetic geometry and the confinement of electrically conducting plasmas," *Phys. Rev. Lett.* **85** (2000) 3416–3419, `physics/0003083`.

[90] J. E. Moore, Y. Ran, and X.-G. Wen, "Topological Surface States in Three-Dimensional Magnetic Insulators," *Phys. Rev. Lett.* **101** (2008) 186805.

[91] Ü. Parts, J. M. Karimäki, J. H. Koivuniemi, M. Krusius, V. M. H. Ruutu, E. V. Thuneberg, and G. E. Volovik, "Phase diagram of vortices in superfluid ^{3} $He - A$," *Phys. Rev. Lett.* **75** (1995) 3320–3323.